NASA TECHNICAL NOTE

NASA TN D-6496

NASA TN D-6496

ANALYSIS OF A COUPLED ROLL-SPIRAL-MODE, PILOT-INDUCED OSCILLATION EXPERIENCED WITH THE M2-F2 LIFTING BODY

by Robert W. Kempel

Flight Research Center
Edwards, Calif. 93523

NATIONAL AERONAUTICS AND SPACE ADMINISTRATION • WASHINGTON, D. C. • SEPTEMBER 1971

1. Report No.	2. Government Accession No.	3. Recipient's Catalog No.
NASA TN D-6496		

4. Title and Subtitle	5. Report Date
ANALYSIS OF A COUPLED ROLL-SPIRAL-MODE, PILOT-INDUCED OSCILLATION EXPERIENCED WITH THE M2-F2 LIFTING BODY	September 1971
	6. Performing Organization Code

7. Author(s)	8. Performing Organization Report No.
Robert W. Kempel	H-633
	10. Work Unit No. 125-19-03-02-24

9. Performing Organization Name and Address	11. Contract or Grant No.
NASA Flight Research Center P.O. Box 273 Edwards, California 93523	
	13. Type of Report and Period Covered: Technical Note

12. Sponsoring Agency Name and Address	14. Sponsoring Agency Code
National Aeronautics and Space Administration Washington, D. C. 20546	

15. Supplementary Notes

16. Abstract

During the 16 glide flights of the M2-F2 lifting body vehicle, severe lateral pilot-induced oscillations occurred on three occasions in the low-angle-of-attack, final-approach, preflare situation. These oscillations were analyzed qualitatively to determine the type and similarity and by a systems analysis to determine the root cause. The analysis was complemented by a piloted simulator study, which verified the results.

The systems analysis revealed the presence of a coupled roll-spiral mode which caused the pilots to generate a closed-loop lateral instability in the low-angle-of-attack, preflare flight region.

A systems analysis, a piloted simulator study, and flight data showed that the addition of a fixed center fin lessened the pilot-induced-oscillation tendencies in the critical flight region.

17. Key Words (Suggested by Author(s))	18. Distribution Statement
Pilot-induced oscillations Coupled roll spiral Lifting body vehicles	Unclassified - Unlimited

19. Security Classif. (of this report)	20. Security Classif. (of this page)	21. No. of Pages	22. Price*
Unclassified	Unclassified	57	$3.00

*For sale by the National Technical Information Service, Springfield, Virginia 22151

ANALYSIS OF A COUPLED ROLL-SPIRAL-MODE, PILOT-INDUCED OSCILLATION EXPERIENCED WITH THE M2-F2 LIFTING BODY

Robert W. Kempel
Flight Research Center

SUMMARY

During the 16 glide flights of the M2-F2 lifting body vehicle, severe lateral pilot-induced oscillations occurred on three occasions in the low-angle-of-attack, final approach, preflare situation. The in-flight pilot-induced oscillations were studied qualitatively, using flight recorded time histories and pilot comments concerning each of the maneuvers. To determine the root cause of the oscillations, a systems analysis was performed using the predicted aerodynamic stability and control derivatives at the conditions at which the pilot-induced oscillation of flight 16 occurred. These studies were complemented by a piloted six-degree-of-freedom simulator study, which verified the results.

The systems analysis with the pilot in the loop related the preflare, low-angle-of-attack, pilot-induced-oscillation tendencies to the formation of a coupled roll-spiral mode which caused the pilots to generate a closed-loop lateral instability. Coordinated use of rudders aggravated the instability. The formation of the coupled roll-spiral mode was attributed to the large effective dihedral, operation in the negative angle-of-attack region, large positive yawing moment due to roll rate, low natural roll damping, and large adverse yawing moment due to aileron deflection.

The M2-F2 vehicle was modified with a fixed center fin and was redesignated the M2-F3. The center-fin modification greatly improved the aileron control characteristics and lateral handling qualities in the low-angle-of-attack, preflare region. A systems analysis and a piloted simulator study of the M2-F3 characteristics indicated that the modified configuration would improve lateral handling qualities. This was confirmed in flight.

The results of this study are in general agreement with the results of other ground and in-flight simulation and theoretical analysis of coupled roll-spiral mode handling qualities.

INTRODUCTION

During the 16 glide flights of the M2-F2 flight-test program, the pilot—vehicle combination experienced severe lateral divergent oscillations on three occasions. The oscillation on the last flight contributed to a gear-up landing in which the vehicle was

extensively damaged. Each of the three oscillations occurred when the pilots were attempting to control bank angle closely at angles of attack below zero, and each oscillation was aggravated by attempts to coordinate aileron control with the rudders.

Reference 1 summarizes, qualitatively, the overall lateral-directional and longitudinal stability and control characteristics of the M2-F2 vehicle for the 16 glide flights. However, dynamic-stability problems involving a pilot—airframe combination cannot be analyzed by considering only a few major static parameters. A systems analysis of the transfer functions involved is required to determine the cause of dynamic-stability problems. The problem of pilot—vehicle combination instability is generally referred to as a pilot-induced oscillation, or PIO. References 2 and 3 treat this subject in detail.

This report identifies the M2-F2 stability and control problem by means of a systems analysis, which provides a quantitative understanding of the problem and its implications. The transfer function of primary interest was the bank-angle-to-aileron deflection. The transfer-function denominator quartic was factored into two second-order factors rather than the more conventional two first-order factors (roll and spiral modes) and a quadratic (Dutch roll mode). The combination of the two first-order factors into a second quadratic has been termed roll-spiral coupling (refs. 4 to 8). Very little flight data are available on vehicles which display roll-spiral coupling; however, reference 4 presents the results of an in-flight investigation of this phenomenon utilizing a variable-stability T-33 aircraft. Other investigators (refs. 5 to 8) limited their analysis to mathematical approaches or simulator studies, or both. In general, these investigators concluded that a vehicle with roll-spiral-coupling characteristics also has degraded lateral handling characteristics.

SYMBOLS

Physical quantities in this report are given in the International System of Units (SI) and parenthetically in U.S. Customary Units. The measurements were taken in U.S. Customary Units. Factors relating the two systems are presented in reference 9.

A...G	coefficients of transfer-function denominator or numerator
a_z	normal acceleration, g units
b	reference span, m (ft)
C_L	lift coefficient, $\frac{\text{Lift}}{qS}$
C_l	rolling-moment coefficient
C_{l_p}	roll-damping derivative, $\frac{\partial C_l}{\partial\left(\frac{pb}{2V}\right)}$, rad^{-1}

C_{l_r}	rolling moment due to yaw rate, $\frac{\partial C_l}{\partial\left(\frac{rb}{2V}\right)}$, rad^{-1}
C_{l_β}	effective dihedral derivative, $\frac{\partial C_l}{\partial \beta}$, deg^{-1}
$C_{l_{\delta_a}}$	aileron-effectiveness derivative, $\frac{\partial C_l}{\partial \delta_a}$, deg^{-1}
$C_{l_{\delta_r}}$	rolling moment due to rudder deflection, $\frac{\partial C_l}{\partial \delta_r}$, deg^{-1}
C_n	yawing-moment coefficient, $\frac{\text{Yawing moment}}{qSb}$
C_{n_p}	yawing moment due to roll rate, $\frac{\partial C_n}{\partial\left(\frac{pb}{2V}\right)}$, rad^{-1}
C_{n_r}	yaw-damping derivative, $\frac{\partial C_n}{\partial\left(\frac{rb}{2V}\right)}$, rad^{-1}
C_{n_β}	directional-stability derivative, $\frac{\partial C_n}{\partial \beta}$, deg^{-1}
$C_{n_{\delta_a}}$	yawing moment due to aileron deflection, $\frac{\partial C_n}{\partial \delta_a}$, deg^{-1}
$C_{n_{\delta_r}}$	rudder-effectiveness derivative, $\frac{\partial C_n}{\partial \delta_r}$, deg^{-1}
C_Y	side-force coefficient, $\frac{\text{Side force}}{qS}$
C_{Y_β}	side-force derivative, $\frac{\partial C_Y}{\partial \beta}$, deg^{-1}
$C_{Y_{\delta_a}}$	side force due to aileron deflection, $\frac{\partial C_Y}{\partial \delta_a}$, deg^{-1}
$C_{Y_{\delta_r}}$	side force due to rudder deflection, $\frac{\partial C_Y}{\partial \delta_r}$, deg^{-1}
$\bar{c}$	mean aerodynamic chord, m (ft)
g	acceleration due to gravity, 9.8 m/sec^2 (32.2 ft/sec^2)

h	altitude, m (ft)
I_X, I_Z	vehicle moments of inertia about the X- and Z-body axes, respectively, kg-m^2 (slug-ft^2)
I_{XZ}	product of inertia, kg-m^2 (slug-ft^2)
$j\omega$	imaginary part of Laplace transform variable, rad/sec
K_I	interconnect ratio, $-\frac{\delta_{r_{K_I}}}{\delta_{a_t}}$, deg/deg
K_{P_φ}	pilot roll gain, ratio of aileron deflection to bank angle error
K_p	roll-damper gain, deg/deg/sec
K_r	yaw-damper gain, deg/deg/sec
K_φ	airframe gain
L_p	dimensionalized roll-damping derivative, $\frac{qSb^2}{2VI_X} C_{l_p}$, sec^{-1}
L_r	dimensionalized rolling moment due to yaw rate, $\frac{qSb^2}{2VI_X} C_{l_r}$, sec^{-1}
L_β	dimensionalized effective dihedral derivative, $\frac{qSb}{I_X} C_{l_\beta}$, sec^{-2}
L_{δ_a}	dimensionalized aileron-effectiveness derivative, $\frac{qSb}{I_X} C_{l_{\delta_a}}$, sec^{-2}
L_{δ_r}	dimensionalized rolling moment due to rudder deflection, $\frac{qSb}{I_X} C_{l_{\delta_r}}$, sec^{-2}
M	Mach number
m	mass, kg (slugs)
N_p	dimensionalized yawing moment due to roll rate, $\frac{qSb^2}{2VI_Z} C_{n_p}$, sec^{-1}
N_r	dimensionalized yaw damping, $\frac{qSb^2}{2VI_Z} C_{n_r}$, sec^{-1}

N_β	dimensionalized directional-stability derivative, $\frac{qSb}{I_Z} C_{n_\beta}$, sec^{-2}
N_{δ_a}	dimensionalized yawing moment due to aileron deflection, $\frac{qSb}{I_Z} C_{n_{\delta_a}}$, sec^{-2}
N_{δ_r}	dimensionalized rudder-effectiveness derivative, $\frac{qSb}{I_Z} C_{n_{\delta_r}}$, sec^{-2}
N_{φ/δ_a}	bank-angle-to-aileron transfer-function numerator
P	period of transient oscillation, sec
p	rolling angular rate, deg/sec
q	dynamic pressure, N/m^2 (lb/ft^2)
r	yawing angular rate, deg/sec
S	reference planform area, m^2 (ft^2)
s	Laplace transform variable, $\sigma + j\omega$, rad/sec
t	time, sec
V	true airspeed, m/sec (ft/sec)
V_i	indicated airspeed, knots
W	weight, kg (lb)
X, Y, Z	vehicle forward, transverse, and vertical body axes, respectively
Y	generalized transfer function
Y_β	dimensionalized side-force derivative, $\frac{qS}{mV} C_{Y_\beta}$, sec^{-1}
Y_{δ_a}	dimensionalized side force due to aileron, $\frac{qS}{mV} C_{Y_{\delta_a}}$, sec^{-1}
Y_{δ_r}	dimensionalized side force due to rudder, $\frac{qS}{mV} C_{Y_{\delta_r}}$, sec^{-1}
α	angle of attack, deg
β	angle of sideslip, deg
Δ	transfer-function denominator

δ_a	aileron deflection, deg
δ_{LS}	pilot's lateral-stick deflection, deg of δ_a
δ_{RP}	pilot's rudder-pedal deflection, deg of δ_r
δ_r	rudder deflection, deg
ζ	damping ratio of second-order response
σ	real part of Laplace transform variable, rad/sec
τ	time constant, sec
φ	angle of bank, deg
$\left\lvert\frac{\varphi}{\beta}\right\rvert$	absolute ratio of bank angle to sideslip angle
ω	frequency, rad/sec
ω_d	undamped natural frequency of Dutch roll mode, rad/sec
ω_{RS}	undamped natural frequency of coupled roll-spiral mode, rad/sec

Subscripts:

c	input signal
d	Dutch roll mode
eff	effective
K_I	interconnect ratio
n	undamped natural frequency
P	pilot
p	roll SAS
R	roll mode
RS	coupled roll-spiral mode
r	yaw SAS
S	spiral mode
SAS	stability augmentation system
t	total
wo	washout

ϵ	error signal
φ	bank-angle transfer-function numerator parameter
0	initial condition

A primed quantity denotes a closed-loop transfer-function parameter. A dot over a quantity denotes the first derivative with respect to time.

VEHICLE DESCRIPTION

M2-F2 vehicle. – The M2-F2 vehicle (figs. 1(a) to 1(d)) was a single-place lifting body configuration with a relatively conventional fighter aircraft type of cockpit

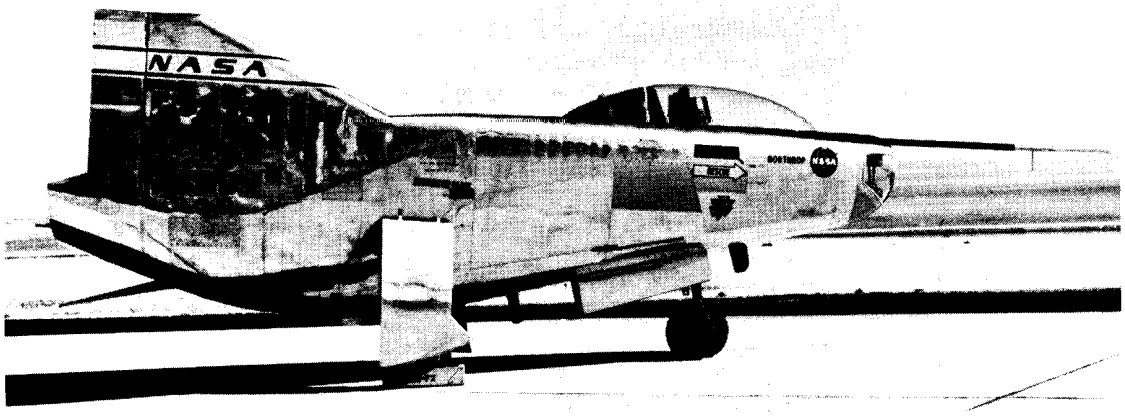

E-14333

(a) Side view.

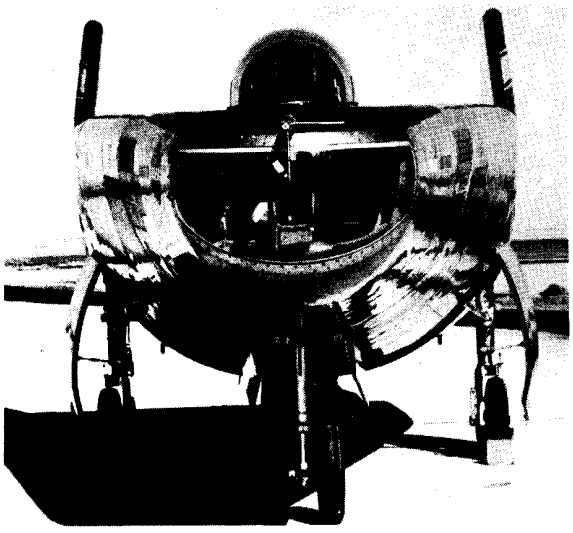

E-14338

(b) Front view.

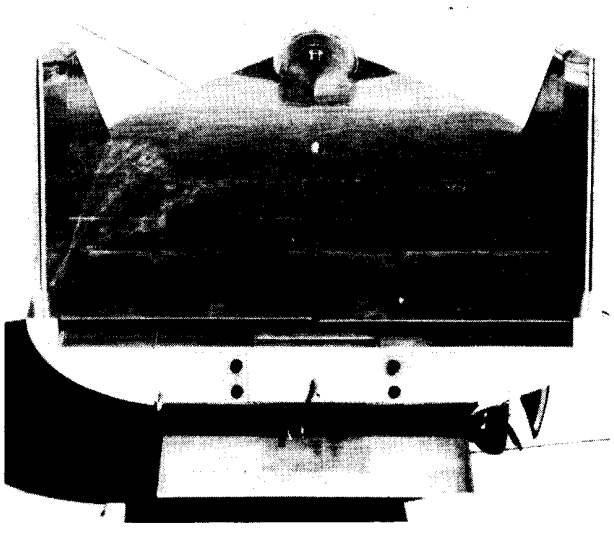

E-14350

(c) Rear view.

Figure 1. M2-F2 vehicle.

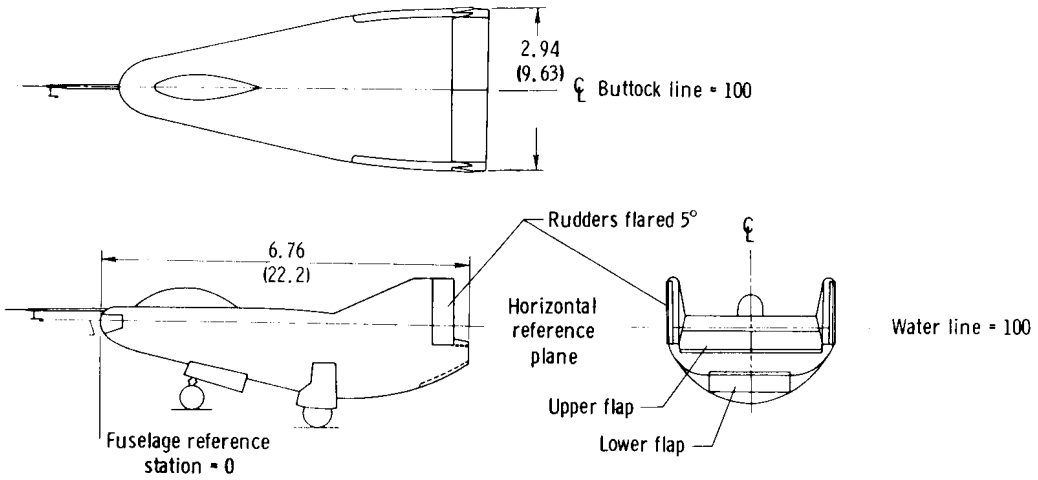

(d) Three-view drawing. Dimensions in meters (feet).

Figure 1. Concluded.

arrangement and cockpit controls (figs. 2(a) and 2(b)). The vehicle was a blunt 13° half cone with tapered afterbody and two aft vertical fins with rudder surfaces on the outboard trailing edges. Pertinent dimensions are given in table 1 and figure 1(d).

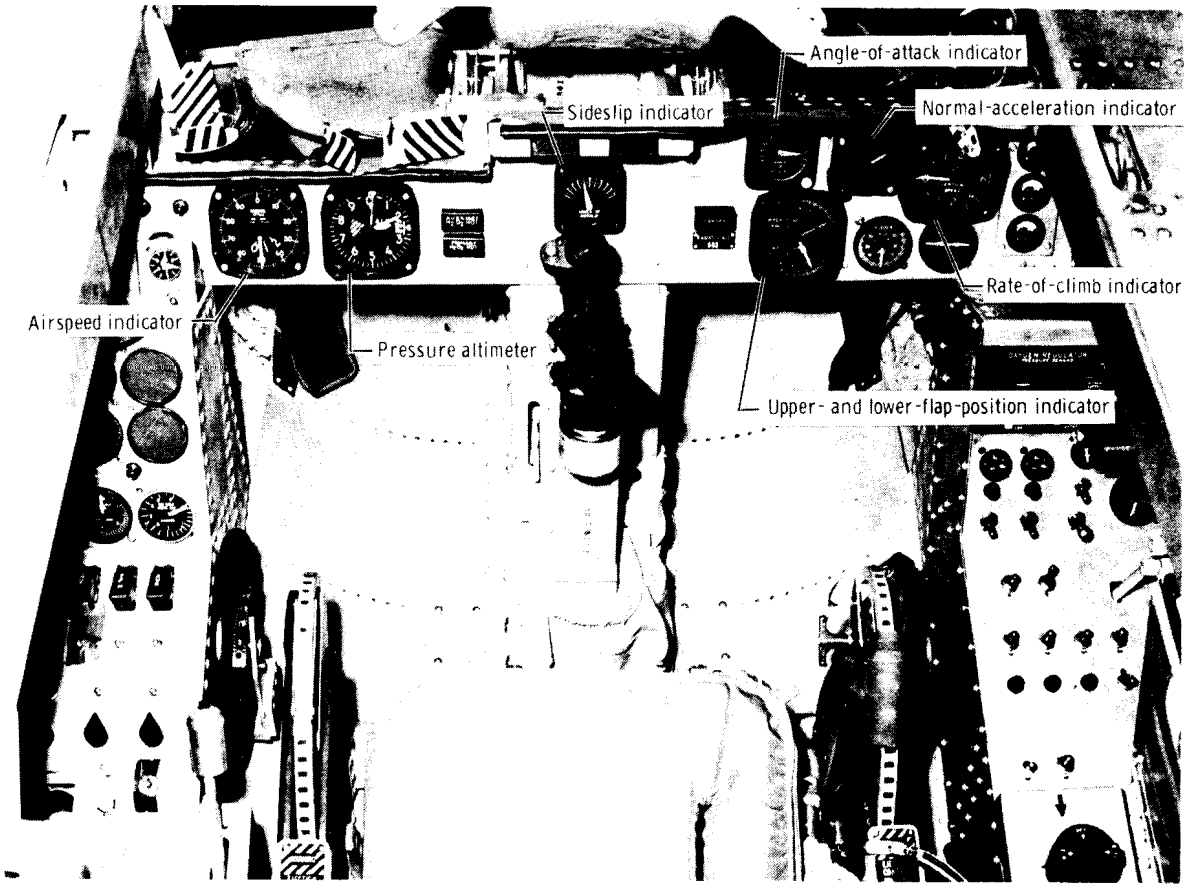

(a) General arrangement. *E-14637*

Figure 2. M2-F2 cockpit arrangement.

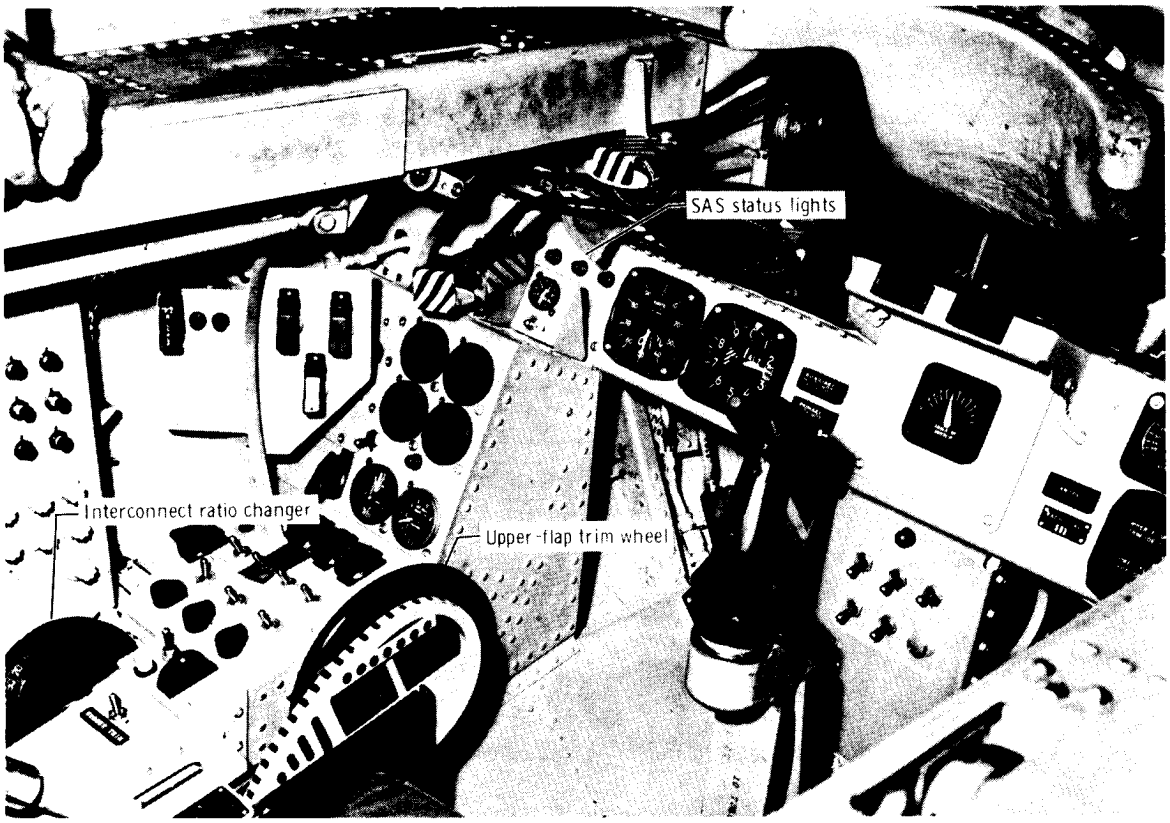

(b) Left-hand console. *E-14630*

Figure 2. Concluded.

Aerodynamic control was provided by upper elevon flaps, a lower flap, and rudders. The rudder surfaces operate about a 5° flared condition. The upper elevon flaps provided coarse longitudinal trim and deflected differentially (aileron deflection) to provide roll control. Roll control was augmented by means of a mechanical aileron-to-rudder interconnect; that is, the rudders were deflected proportionally to aileron deflection. The interconnect-ratio changer was on the pilot's left-hand console (fig. 2(b)). The ratio of aileron-to-rudder deflection could be selected from zero to 1.25; however, it was generally set at approximately 0.5.

The surfaces were actuated by hydraulic systems that accepted commands from both the pilot and the stability augmentation system (SAS). Stick and pedal-force feel were provided the pilot by coil-spring bungees which produced a force proportional to stick or rudder-pedal position (table 2).

A simple three-axis rate feedback stability augmentation system (fig. 3) provided damping augmentation about all three axes. The feedback signals were provided by conventional rate gyros. SAS gains were selected by the pilot and were fixed unless he manually changed the switch position. The SAS control panel was on the pilot's left-hand console (fig. 2(b)). The roll and yaw rate signals were fed back to mechanical actuators which actuated the aileron and rudder, respectively. The roll and yaw signals were modified by a high-pass filter, that is, a washout filter. The purpose of the washout filter was to cancel damper signals to the control surfaces when the angular

rates approached steady states. The washout filter was used to improve the vehicle's handling qualities during turn maneuvers. The washout time constant, τ_{wo}, was 1.75 seconds. Without the washout filter, the vehicle tended to be very sluggish. Reference 10 presents additional information on the flight control system.

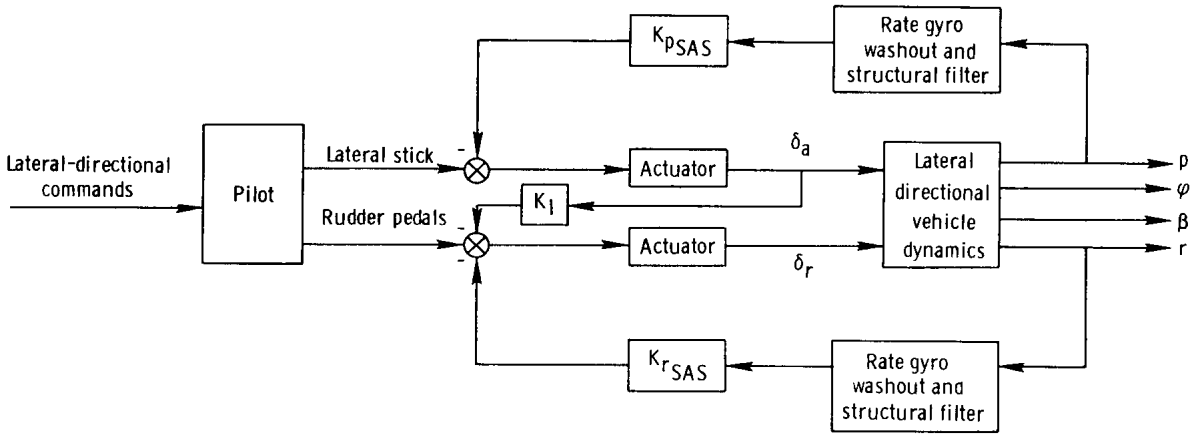

Figure 3. Block diagram of M2-F2 lateral-directional flight control system.

Basic cockpit instrument displays of airspeed, altitude, angle of attack, angle of sideslip, normal acceleration, and control-surface positions were provided (figs. 2(a) and 2(b)). After flight 13, a three-axis attitude indicator was installed in place of the sideslip indicator shown in figure 2(a). Sideslip was then displayed on the vertical needle of this instrument.

The pilot's stick and rudder-pedal characteristics are presented in table 2, together with surface rate limits. Corresponding control-surface deflections and SAS authorities are presented in table 1.

M2-F3 vehicle. - After the M2-F2 landing accident, the vehicle was rebuilt and modified and was designated the M2-F3. The modified vehicle incorporates a fixed center dorsal fin (fig. 4).

INSTRUMENTATION

Standard sensors were used to determine all flight quantities of interest. Data were acquired by means of a pulse code modulation telemetry system with digital recording on standard magnetic tape at the ground station. The sampling rate was 200 per second. Accuracies of recorded quantities are estimated to be within 2 percent of the full-scale system (table 3). Bank-angle measurements beyond ±45° were generally inaccurate because of the nonlinear output of the attitude gyro.

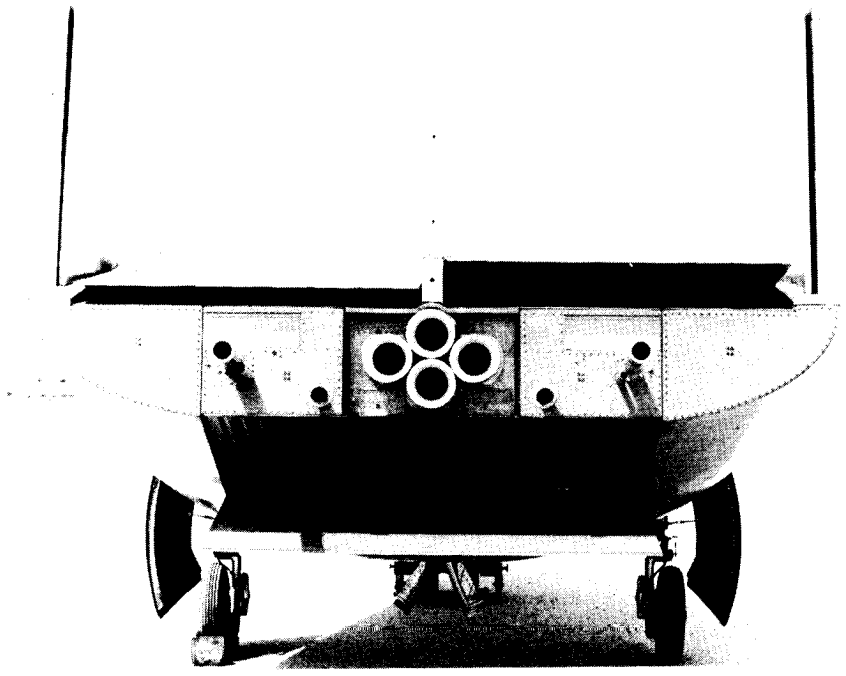

E-21534

Figure 4. Rear view of the M2-F3 vehicle.

FLIGHT TESTS

Test Methods

After the M2-F2 lifting body was launched from a B-52 airplane at about 13,716 meters (45,000 feet) altitude and a Mach number of about 0.6, flight-test maneuvers were performed during gliding descent to assess the stability, control, and handling characteristics of the vehicle. Pilot ratings of the handling qualities of the vehicle, based on a modified Cooper (ref. 11) rating scale (table 4), were obtained immediately after each flight. The pilots were thoroughly familiar with the desired flight plan and the predicted handling qualities of the vehicle as a result of practicing on a complete six-degree-of-freedom, fixed-base simulator with instruments similar to those of the actual flight vehicle. An attitude indicator provided basic attitude information. Upsets such as turbulence and cross winds were not included in the simulation.

Flight Envelope

A typical M2-F2 ground track is shown in figure 5. Figure 6 is a time history of a typical M2-F2 glide flight. Indicated airspeeds ranged from about 165 knots at launch to 310 knots prior to the flare and landing. Landing touchdowns were made at velocities as low as 155 knots indicated airspeed. The maximum Mach number was approximately 0.70, and the maximum dynamic pressure was approximately 14,840 newtons/meter^2 (310 pounds/foot^2). Angles of attack from 16° to -5° were flown, and normal

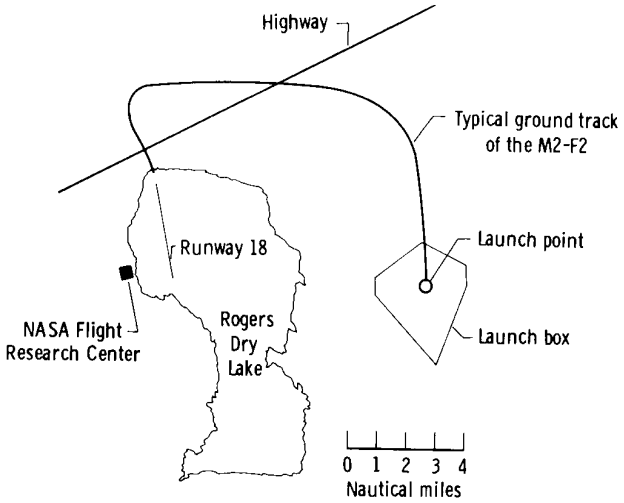

Figure 5. Typical M2-F2 ground track.

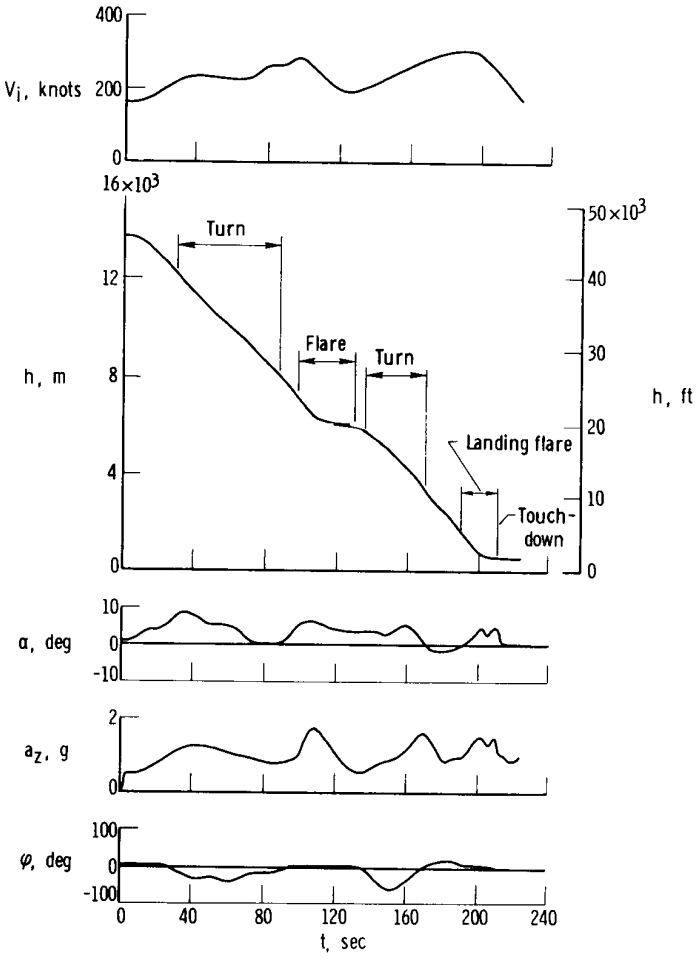

Figure 6. Time history of a typical glide flight of the M2-F2 vehicle.

accelerations as high as 2g were reached. Turn maneuvers were made with bank angles of 60° or less; however, bank angles in excess of ±100° were encountered during inadvertent roll oscillations.

Figure 7 is a typical M2-F2 flare and landing profile. The approach and landing technique used for unpowered landings required that a relatively high airspeed (approximately 300 knots) be maintained until the flare altitude of 305 meters (1000 feet) above ground level was reached. At this altitude, approximately a 1.5g flareout was initiated to bring the vehicle to near-level flight at 30.5 meters (100 feet) altitude. Once the vehicle was at flare conditions, deceleration was rapid because of the high drag of this configuration. To maintain an indicated airspeed of 300 knots, it was necessary to operate in the zero to -3° angle-of-attack range because $C_L = 0$ occurred at $\alpha \approx -6°$ and maximum lift-to-drag ratio at $\alpha \approx 6°$.

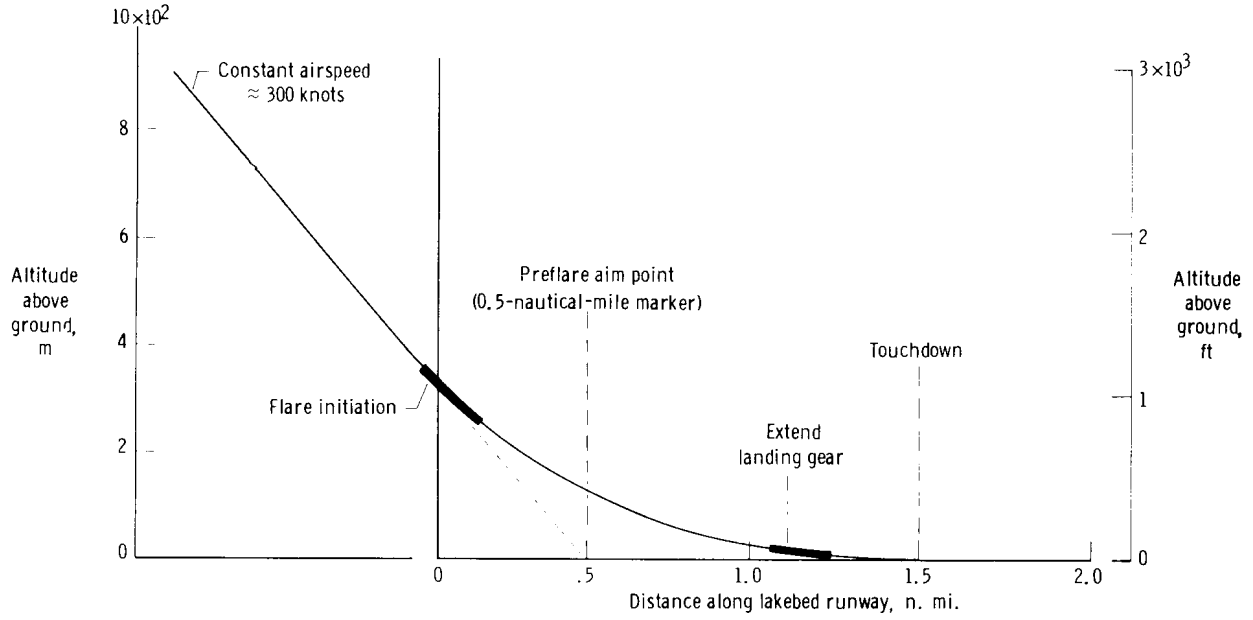

Figure 7. Typical M2-F2 flare and landing profile.

RESULTS AND DISCUSSION

Data from M2-F2 flights 1, 10, and 16, on which severe lateral divergent oscillations occurred, were analyzed qualitatively on the basis of flight time histories and corresponding pilot comments and pilot ratings. Observations are presented concerning the similarity of each of the divergent maneuvers, that is, the method of control used prior to and during the maneuvers, and recovery from the maneuvers. A systems analysis was made to determine the root cause of the PIO problem and its implications. To complement this analysis a piloted six-degree-of-freedom simulator was used to verify and correlate the quantitative results. A similar analysis of a proposed modification to the basic M2-F2 airframe was made to assess the suitability of the proposed "fix."

M2-F2 Lateral Controllability

Flight. – Figures 8(a) and 8(b) are flight time histories of the PIO which occurred during a turn and pushover to the final approach on the first flight of the M2-F2 vehicle.

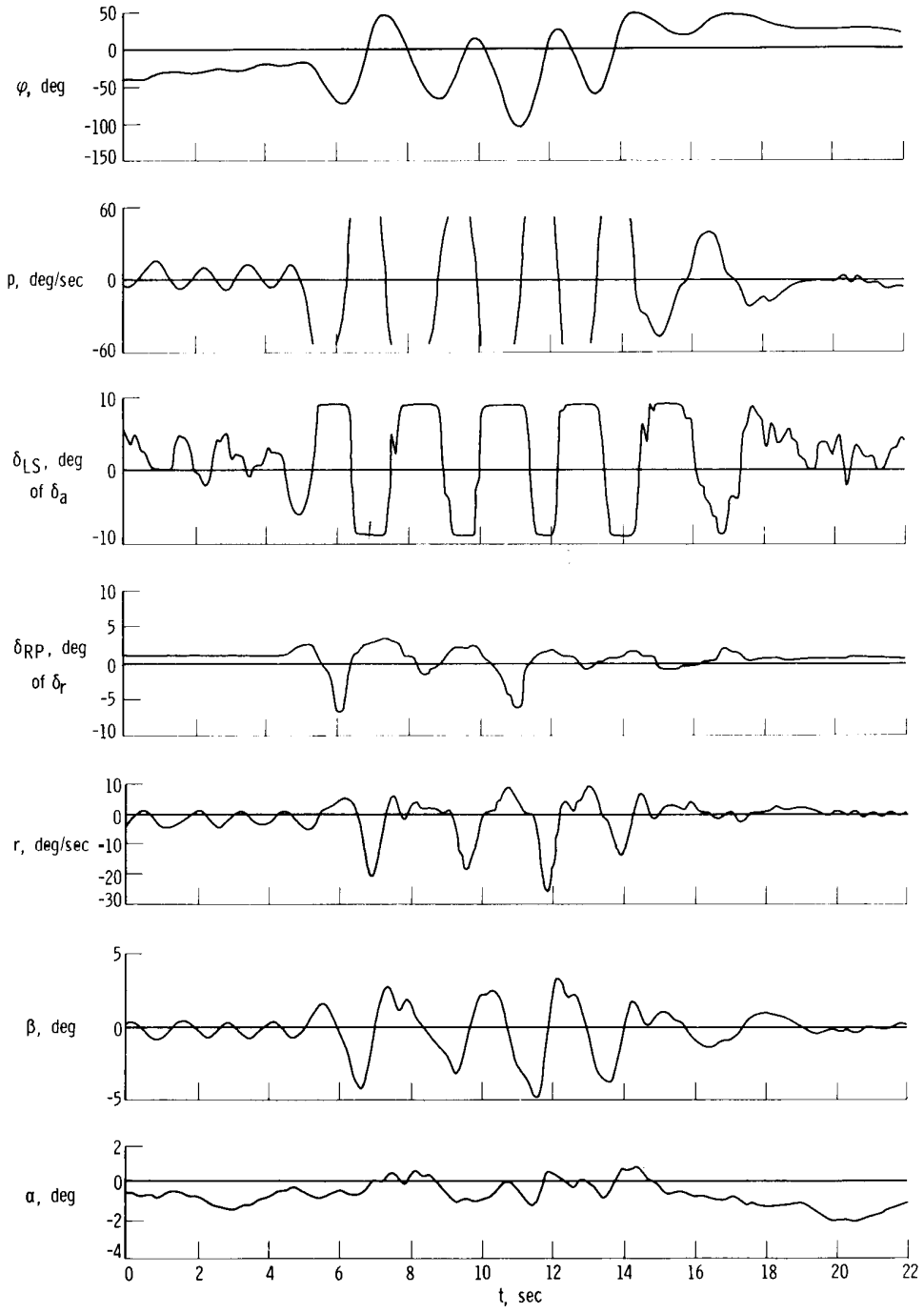

(a) Pilot's input and vehicle response.

Figure 8. Time history of pilot-induced lateral-directional oscillation on M2-F2 flight 1. M = 0.48; h = 2830 m (9275 ft) to 1678 m (5500 ft); K_p = 0.6; K_r = 0.6.

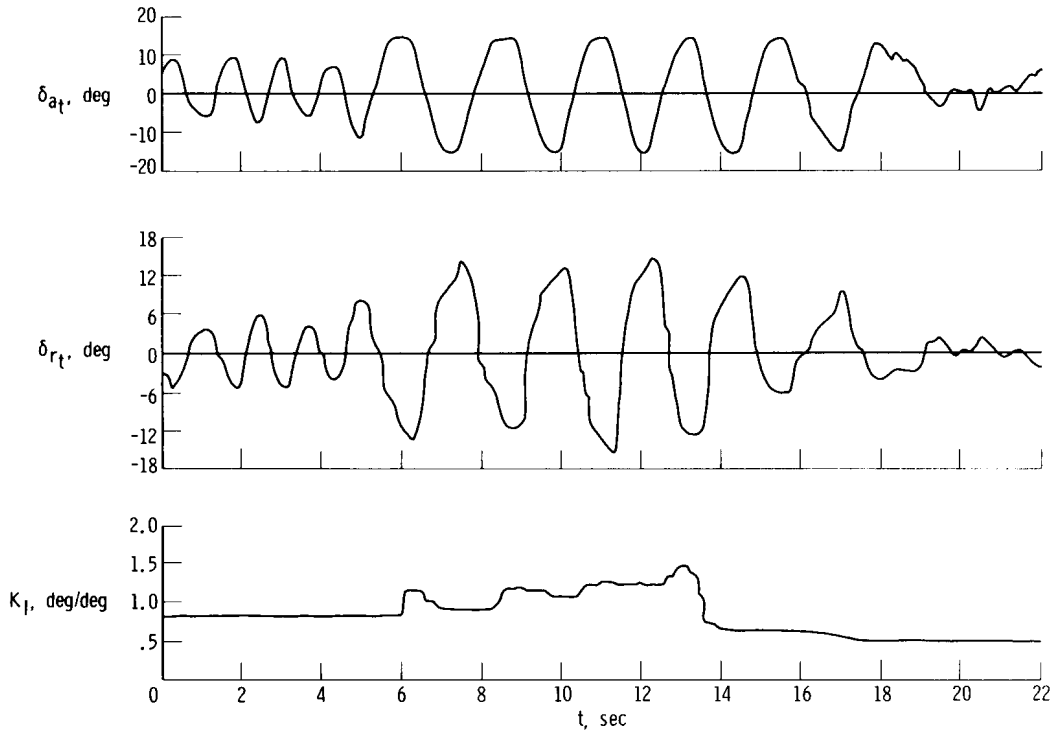

(b) Control and interconnect inputs.

Figure 8. Concluded.

The pilot commented: "I tried to start a turn, but I had the interconnect ratio down about 0.4, and it just didn't seem like I was getting anything. So I cranked it back up to 0.6 and got the turn started; I used a little rudder to get it started. Then during the pushover I got into this lateral-directional thing [oscillation]. It's just much too sensitive at this interconnect ratio at the low angles of attack. Every time I would push over, I would be right in it. So, again, as soon as I got into it I thought, well, I'll crank the interconnect ratio down. I started cranking, but at this time I was cranking the wrong way and as it got worse I kept cranking and finally looked down and I had an excess of 1.0. Bank angles were in excess of 90° at a fairly high rate from one side to the other. When I noticed how high I had gone on interconnect ratio, I cranked it back down and let go of the stick, and the airplane took over and it damped out very readily after that."

The PIO on this maneuver was attributed to a high interconnect ratio. However, figure 8 shows that a divergence developed before the pilot actuated the interconnect. As a left bank angle of approximately 20° was approached, at angles of attack below zero, a relatively large left aileron and rudder input was commanded, followed immediately by a larger right aileron and rudder input. At this point the PIO was fully developed and was sustained through four cycles. Although the interconnect was at a relatively high setting initially, 0.8, this control was actuated by the pilot after the PIO started. Figure 9 presents the simulator-determined interconnect versus angle-of-attack control boundaries (ref. 1). Although a PIO boundary was indicated, no attempt was made to specifically identify the cause of the PIO problem.

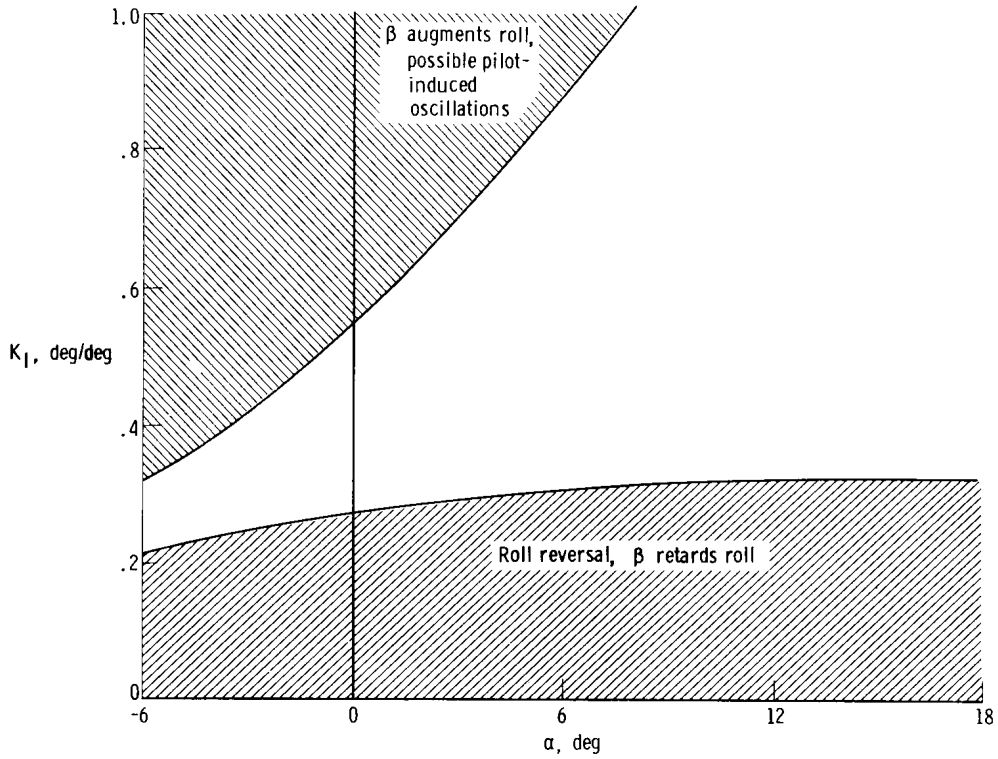

Figure 9. M2-F2 simulator-predicted regions of basic M2-F2 lateral-control problems as function of angle of attack and aileron-to-rudder interconnect ratio. M = 0.4.

Figures 10(a) and 10(b) are flight time histories of the PIO which occurred after an attempted dampers-off aileron pulse on the tenth glide flight of the M2-F2 vehicle. The pilot comments were: "I'd like to make a note here and a general comment about this second leg where the pushover and aileron pulse at zero degree angle of attack were accomplished. In the pushover, in an attempt to stabilize at zero degree alpha, considerable pilot attention is required to get to the desired longitudinal and lateral-directional conditions. Small Dutch roll oscillations are apparent. During recovery from the aileron pulse maneuver with roll and yaw dampers on, attempts were made to reduce the left roll, both the bank angle and the roll rate. An immediate roll PIO developed and continued through three cycles. I was already in the left bank or left roll because of the aileron pulse and it [the vehicle] went immediately to the right, back to the left, and then to the right. The divergent roll and yaw was stopped only by releasing all controls, followed by back stick to increase alpha; thereafter, the vehicle settled down well and I was able to recover. I think it was more my input that caused the thing than anything else. It was obvious that I was trying to damp it out, and you just can't stay with it. The only suggestion I have, as far as anybody flying it is concerned and when we do this again, is to go ahead and turn the dampers back on but concentrate more on staying off the controls until things are damped out and then recover from that position. Put in pitch control first, no matter what your bank angle is."

Figure 10 shows that the initial roll rate and bank angle were to the left at the time the aileron was pulsed to the left. The pilot thought that he had to recover from the divergent roll maneuver; however, an immediate PIO resulted. Control was regained only after angle of attack was increased and pilot control activity was relaxed. The overall maneuver was rated 4, longitudinal control was rated 3, and lateral-directional control was rated 5.

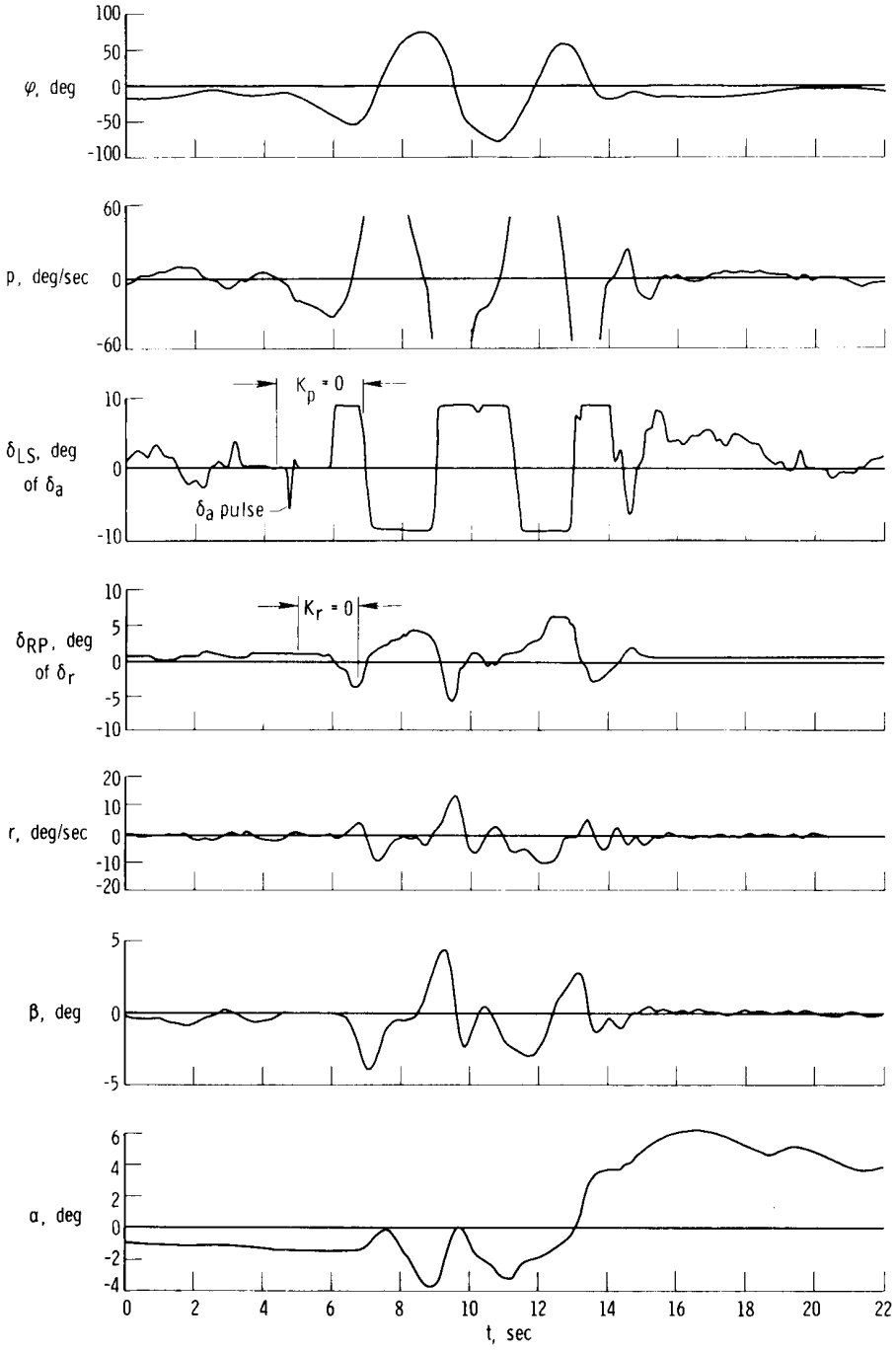

(a) Pilot's input and vehicle response.

Figure 10. Time history of pilot-induced lateral-directional oscillation on M2-F2 flight 10. M = 0.61; h = 7020 m (23,000 ft) to 5800 m (19,000 ft); K_p = 0.4 and K_r = 0.6 except as noted; K_I = 0.49.

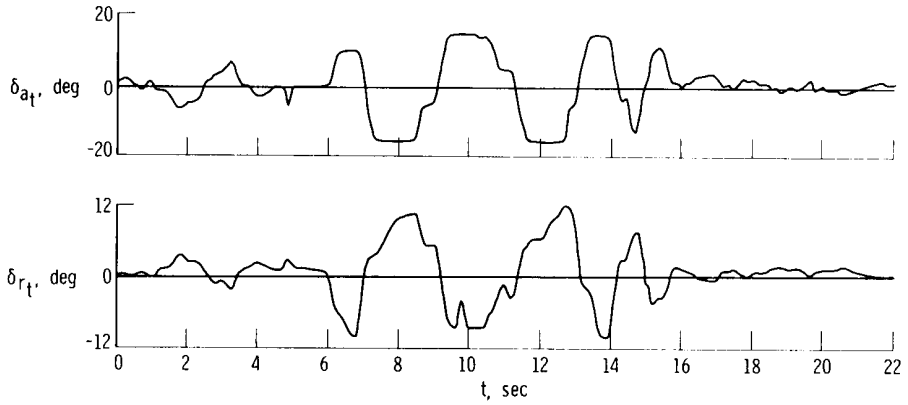

(b) Control inputs.

Figure 10. Concluded.

Figures 11(a) and 11(b) are flight time histories of the PIO which occurred at the rollout of the turn to final approach as the bank angle became zero on the sixteenth, and last, flight of the M2-F2 vehicle. Even though control was regained, this oscillation and other distractions contributed to a gear-up landing in which the vehicle was extensively damaged. The pilot comments concerning this maneuver were: "I started to turn in and, as called out ahead of time, had elected to land somewhat across runway 18 rather than down 18 to take out a little bit of the crosswind. I still had this plan in mind and turned in about the second line from the west on 18, knowing that the winds were going to blow me to the east a little bit, and then planned on angling across the lines and being on the lines for my landing, to use those for a landing reference. I was well on my descent and picking up speed at very low angle of attack. In the final approach, as I went into the final turn, I wasn't getting the turn rate that I wanted so I turned the interconnect up to 0.45 and then continued the turn. I was well established in my glide, very low angle of attack, picking up my airspeed, and had the feeling that I would land just slightly short of the 2-mile point angling across the runway. Everything was going normally with no problems, then suddenly at 5000 to 7000 feet, with no warning at all, I experienced very high roll accelerations as a divergent Dutch roll type of maneuver developed. Roll rates were extremely high and, from experience with high roll rate maneuvers in the F-100, I would say rates in excess of 220 degrees per second. This maneuver was disorienting, and I pulled back on the stick to increase angle of attack, trying to damp it out. The first thing that entered my mind was that the interconnect was too high so, as soon as I was able to get hold of the situation, I checked my interconnect; it was 0.45, about where I wanted it. The corrective action of pulling back on the stick damped out the maneuver."

From figure 11 it can be seen that the vehicle appeared to be rolling out of the turn in a normal manner at time zero. As the vehicle rolls to the right through approximately 20° left bank angle, the pilot commands left aileron input in anticipation of reaching a "wings level" attitude. The vehicle continues to roll through zero bank angle very slightly to the right and begins to roll back to the left. In an attempt to maintain zero degree bank angle, the pilot counters with right stick and a small coordinated rudder input. The vehicle responds to this command as it begins to roll back to the right. The pilot again attempts to maintain "wings level" with a larger left stick input ($t > 6$ sec), followed again by a coordinated rudder input. After $t \approx 7$ seconds, both roll rate and bank angle were diverging, and, as larger coordinated aileron and rudder inputs were commanded, the PIO developed fully and was sustained for approximately 9 seconds.

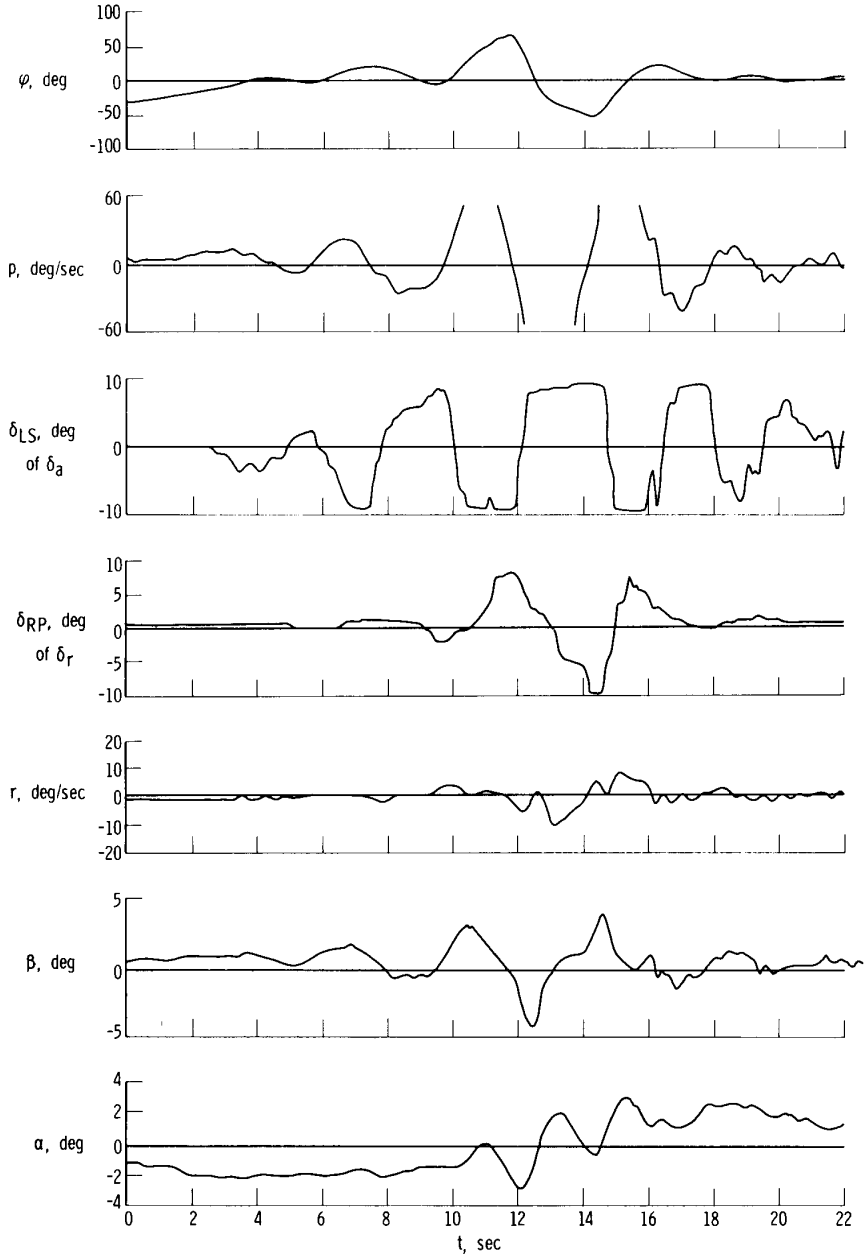

(a) Pilot's input and vehicle response.

Figure 11. Time history of pilot-induced lateral-directional oscillation on M2-F2 flight 16. M = 0.48; h = 2620 m (8577 ft); V = 159.5 m/sec (523 ft/sec); q = 12,100 N/m^2 (253 lb/ft^2); K_p = 0.2; K_r = 0.4; K_I = 0.45.

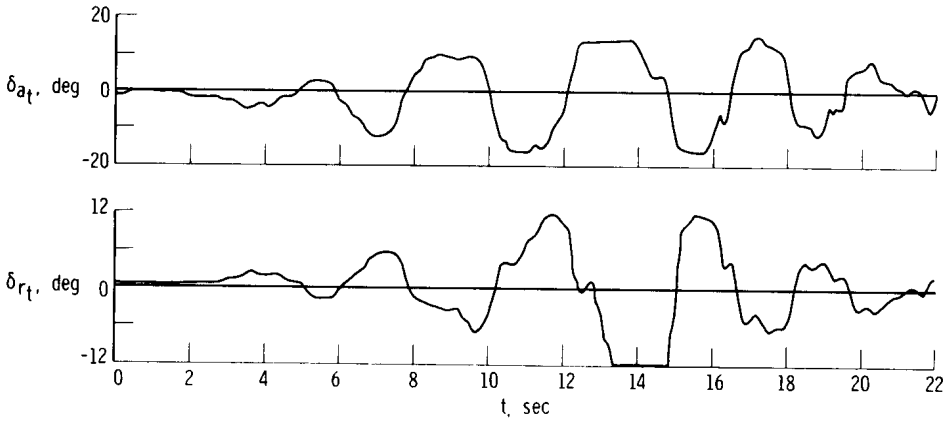

(b) Control inputs.

Figure 11. Concluded.

The first cycle produced a right bank angle of about 16° and a left bank angle of 6°. During the second cycle, bank angles of at least 90° right and 120° left were experienced. (Maximum values were obtained from photographic coverage inasmuch as instrumentation was not adequate beyond $\varphi = 45°$.) In the third cycle bank angles of about 20° right were reached, and then a near-level attitude was regained as the vehicle was recovered to stabilized flight. During the oscillation, roll rates greater than 50 degrees per second were indicated. Recovery was made in a manner similar to that used to recover from the PIO experienced in flight 10 (fig. 10), that is, after angle of attack was increased and pilot control was relaxed.

To complete the qualitative analysis of the flight data, the pilot comments from M2-F2 flight 15 are included. The flight plan was similar to that of the sixteenth flight. The pilot made the following comments:

"I pushed on over for the first [longitudinal] pulse, and, when I got down around 5° angle of attack, I could detect a lateral trim change. I trimmed laterally a little bit, with no results. There just wasn't any way I was going to get good lateral trim. I couldn't understand what such a trim change was and what it was all about and why I couldn't trim it out, so I gave up on that and just pushed on over to zero degree alpha. I thought I might be getting my feet on the rudders because I was getting this sensation I think all of us have talked about as nibbling [lateral-directional nibbling] when you get down around zero degree angle of attack.

"The second turn, coming around the corner at very low angle of attack, I was experiencing small lateral perturbations. At that altitude it's not really much of a problem, but it is disconcerting because of the lateral problems I had previously. I am sure that without those it would probably be a pilot rating of 2 or 3 overall; however, I am going to give it an overall rating of 5.

"On the high-speed approach as I got closer to the ground, I still had the lateral problems cropping up, and I would give that a rating of 6. There again it is all due to the lateral problem.

"The vehicle appears to be very stable longitudinally; it was only hard to control laterally. Longitudinal control was quite positive. The pilot workload on this flight was probably higher than on any of the others--this was due to the lateral problems I had."

The preceding qualitative analysis of the M2-F2 flight time histories and corresponding pilot comments showed that:

Operation in the near-zero and below angle-of-attack region was critical because of the strong lateral PIO tendencies. Normal operation of the stability augmentation system and flight control system did not preclude these tendencies.

Each of the four program pilots was critical of the lateral handling qualities in the near zero and below angle-of-attack region. Three of the pilots experienced a severe lateral PIO. The PIO subsided when control activity decreased, particularly rudder-pedal activity, or when control activity was decreased and angle of attack was increased.

Systems analysis of PIO. – The maneuvers shown in figures 8, 10, and 11 represent a complex control situation. In each of the pilot-induced oscillations, aileron control was coordinated with rudder control in the attempted recovery. In the following systems analysis the pilot is assumed to operate as a pure gain, using aileron only to control bank angle. With these simplifying assumptions, operation in the low-angle-of-attack region is shown to produce an unacceptable situation.

The equations of motion used in this study for both the simulator and systems analysis are presented in appendix A. The development of the equations of motion and associated transfer functions is not discussed, inasmuch as it can be found in any basic aircraft stability and control document, for example, reference 7.

The basic airframe transfer function which relates bank angle to aileron is

$$\frac{\varphi}{\delta_a} = \frac{N_{\varphi/\delta_a}}{\Delta} \tag{1}$$

which can be expressed as

$$\frac{\varphi}{\delta_a} = \frac{A_\varphi s^2 + B_\varphi s + C_\varphi}{As^4 + Bs^3 + Cs^2 + Ds + E} \tag{2}$$

The numerator of this transfer function generally remains a second-order factor. The denominator can normally be factored into two first-order factors and a quadratic. Normal factorization of this transfer function is illustrated in the following equation:

$$\frac{\varphi}{\delta_a} = \frac{K_\varphi(s^2 + 2\zeta_\varphi\omega_\varphi s + \omega_\varphi{}^2)}{(s + \frac{1}{\tau_R})(s + \frac{1}{\tau_S})(s^2 + 2\zeta_d\omega_d s + \omega_d{}^2)} \tag{3}$$

The coefficients of this transfer function are presented in appendix A in terms of their constituent inertial characteristics and aerodynamic derivatives as well as modal response characteristics.

The basic airframe characteristic equation is given by the transfer-function denominator, which determines the basic vehicle transient response and stability characteristics. The first first-order factor is normally referred to as the roll mode because it has a dominant effect on the rapid bank-angle response. The second first-order factor is called the spiral mode and has a dominant effect on the relatively long term bank-angle and heading (spiral) response. The second-order factor represents the Dutch roll mode, which is normally an oscillatory mode of relatively short period involving all lateral-directional variables.

Traditionally, when lateral-directional response characteristics of high-performance aircraft have been found to be deficient, the Dutch roll mode has been the primary contributor. Aerodynamicists usually attempt to design configurations which will have acceptable Dutch roll dynamics; however, this goal is not always attained and this mode must be altered by the introduction of a device such as a yaw rate damper. The roll mode, for higher aspect ratio designs, is usually a well damped, aperiodic mode and not generally troublesome. For high-performance, low-aspect-ratio configurations the roll mode may become sufficiently lightly damped to cause the lateral response of this mode to be unacceptable and require a roll rate damper. The spiral mode is usually a near neutral or slightly unstable aperiodic mode and can be a problem if it becomes too unstable.

The bank-angle-to-aileron transfer function for the M2-F2 vehicle without SAS and interconnect was found to factor into two first-order factors in the numerator and two second-order factors in the denominator. The transfer function is of the form

$$\frac{\varphi}{\delta_a} = \frac{K_\varphi(s + \frac{1}{\tau_{\varphi_1}})(s + \frac{1}{\tau_{\varphi_2}})}{(s^2 + 2\zeta_{RS}\omega_{RS}s + \omega_{RS}^2)(s^2 + 2\zeta_d\omega_d s + \omega_d^2)} \tag{4}$$

The two first-order factors in the numerator occur primarily because of the very high adverse aileron yawing-moment derivative, $-N_{\delta_a}$, and large effective dihedral derivative, L_β. With the inclusion of the interconnect, the numerator becomes a second-order factor, with the resulting zeros in the left-hand plane. The transfer function is now of the form

$$\frac{\varphi}{\delta_a} = \frac{K_\varphi(s^2 + 2\zeta_\varphi\omega_\varphi s + \omega_\varphi^2)}{(s^2 + 2\zeta_{RS}\omega_{RS}s + \omega_{RS}^2)(s^2 + 2\zeta_d\omega_d s + \omega_d^2)} \tag{5}$$

The denominator of this expression consists of two second-order factors and describes the situation which generally exists at all angles of attack for the M2-F2 vehicle with SAS off. Thus the roll mode has become sufficiently lightly damped that it has coupled with the spiral mode to form a second oscillatory mode, the coupled roll-spiral mode. The period of this mode is generally long compared with that of the Dutch roll mode, and it has sometimes been called the lateral phugoid. In reference 7, Ashkenas and McRuer generally related the possible existence of this mode to configurations with large effective dihedral and negative product of inertia, L_β and I_{XZ}, and

positive yawing moment due to roll rate, N_p. Physically, these conditions could be satisfied on configurations with high-mounted wings at high sweep angles (low aspect ratio) and high rear-mounted fins.

Figures 12(a) and 12(b) present the computed zeros and poles for the M2-F2 vehicle without SAS at the flight conditions of figure 11. Included are the zeros for the condition when the interconnect is set at zero and 0.45. (The washout filter characteristics are not considered at this point.) With the interconnect set at 0.45, the zeros become complex in the left-hand plane. As the angle of attack decreases, the Dutch roll mode decreases in frequency, as would be expected, and increases in damping. The coupled roll-spiral mode exists at all angles of attack (fig. 12(b)). As the angle

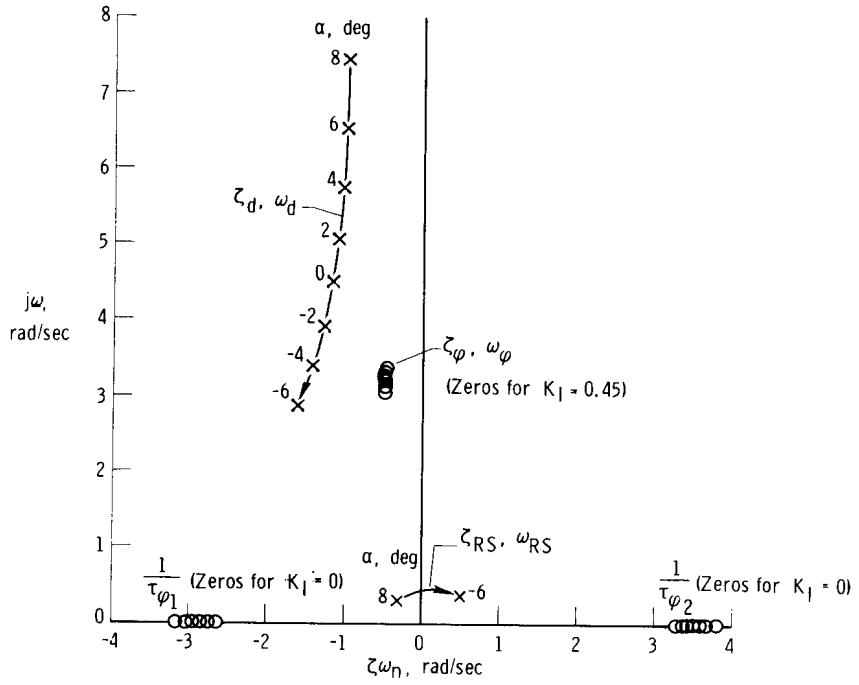

(a) Bank-angle zeros and Dutch roll poles.

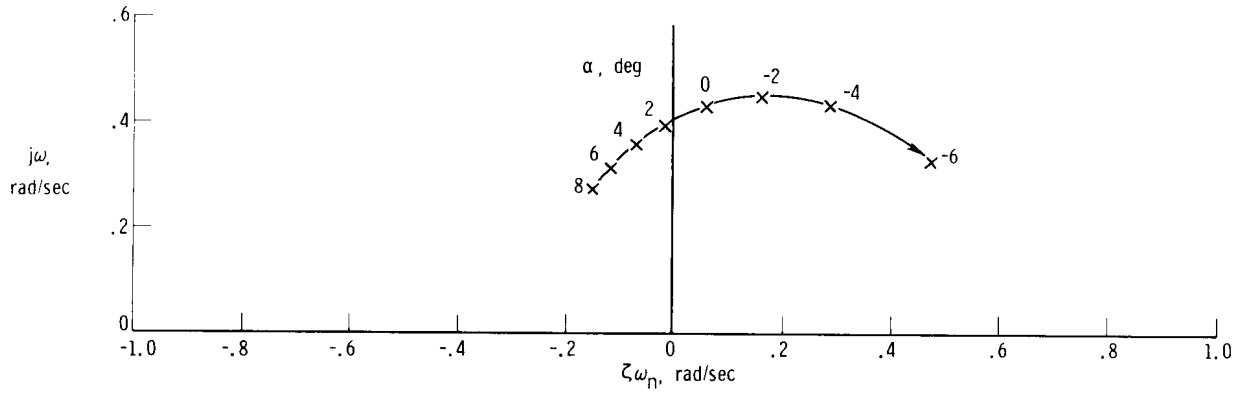

(b) Coupled roll-spiral mode poles.

Figure 12. Complex plane plot of the SAS-off open-loop bank-angle-to-aileron transfer function zeros and poles as a function of angle of attack for the M2-F2 at K_I = 0 and 0.45. M = 0.48; V = 159.5 m/sec (523 ft/sec); q = 12,100 N/m^2 (253 lb/ft^2).

of attack is decreased, the coupled roll-spiral-mode pole migrates toward the imaginary axis (neutral stability) and at angles below approximately 2° becomes unstable. At -6° angle of attack the time for a disturbance of this mode to double amplitude is on the order of 1.5 seconds. From a stability standpoint this situation is obviously unacceptable.

The predicted aerodynamic characteristics of the M2-F2 vehicle were obtained from both small-scale and full-scale wind-tunnel tests (ref. 12). The predicted dimensionless stability and control derivatives are presented in table 5.

The inertial characteristics used in this study are presented in table 1. The mass distribution of the M2-F2 vehicle was characterized by a relatively low roll inertia, as compared with the yaw inertia, and a large negative inclination of the principal axis. The ratio of yaw-to-roll inertia was approximately 6.5, and the ratio of the product of inertia to roll inertia was approximately -0.58.

The dimensionalized aerodynamic derivatives, coefficients of the transfer function, transfer function zeros and poles, and dynamic characteristics were computed by using a digital computer. The computed characteristics are at the flight conditions of figure 11. The dimensionalized aerodynamic derivatives and coefficients of the transfer function for angles of attack of 8° to -6° are presented in table 6.

For the same conditions with inner roll and yaw rate feedback loops closed, that is, with roll and yaw damping augmentation, the equivalent derivative method was used. (See appendix B.) Tables 6 and 7 present the dimensionalized aerodynamic derivatives, coefficients of the transfer function, and the zeros, poles, and modal response characteristics. Figure 13 presents the computed zeros and poles for $K_p = 0.2$,

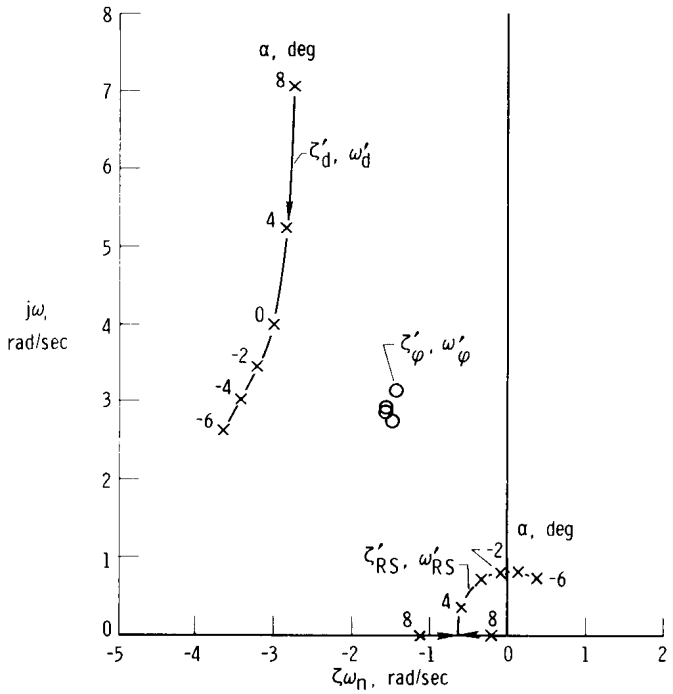

Figure 13. Complex plane plot of the SAS-on open-loop bank-angle-to-aileron transfer-function zeros and poles as a function of angle of attack for the M2-F2. M = 0.48; V = 159.5 m/sec (523 ft/sec); q = 12,100 N/m^2 (253 lb/ft^2); K_p = 0.2; K_r = 0.4; K_I = 0.45.

$K_r = 0.4$, and $K_I = 0.45$. The zeros are complex and have been shifted to the left, as compared with the unaugmented condition. At 8° angle of attack there are distinct roll and spiral modes. At this point the spiral mode is stable and the roll mode is relatively lightly damped. As the angle of attack is decreased, the roll- and spiral-mode poles converge and split from the real axis as they couple to form the roll-spiral mode. As the angle of attack decreases, the coupled roll-spiral-mode pole migrates toward the right-hand plane and becomes unstable between -2° and -4° angle of attack. To attain 300 knots indicated airspeed in the preflare condition, it was necessary for the M2-F2 vehicle to operate in this angle-of-attack region (fig. 6).

To take the analysis of the M2-F2 PIO problem one step further, it is necessary to introduce the pilot and control system high-pass filter characteristics into the closed-loop situation. Figure 14 is a block diagram of the M2-F2 closed-loop system which is analyzed in the following sections. Reference 3 presents a rationale concerning the causes and analysis of PIO problems and classifies them into three distinct types. Types II and III involve system nonlinearities and, as such, require sophisticated analysis. The M2-F2 PIO problem was determined to be in the type I category; that is, the oscillations were determined to be caused by linear pilot—vehicle coupling. The pilot describing function was assumed to be a pure gain; that is, no natural lag or pilot equalization was considered. This is not to say that the pilot(s) closed the lateral control loop in this manner; however, for pure oscillations this approximation is valid.

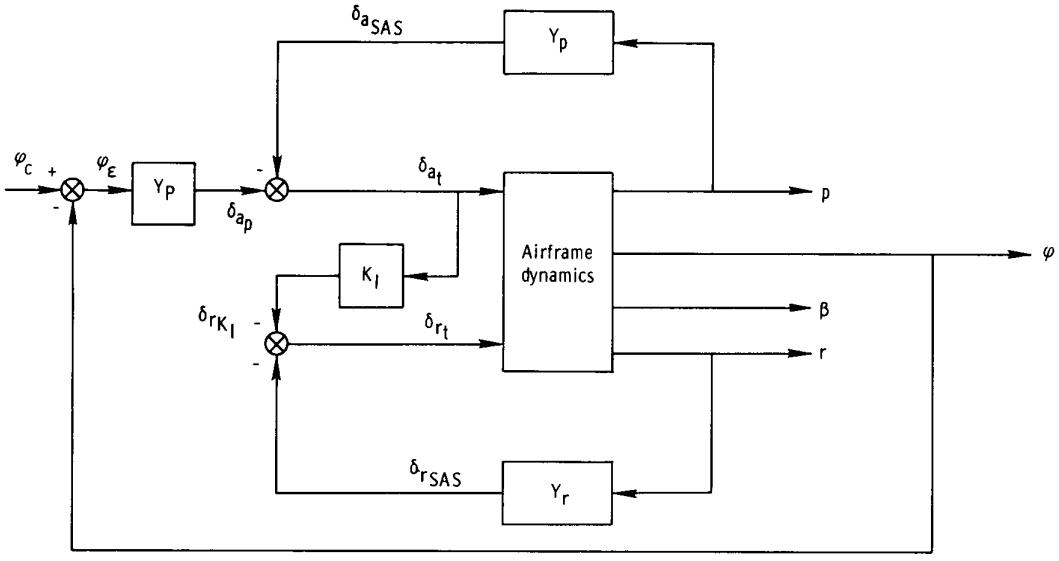

Figure 14. Block diagram of M2-F2 vehicle-pilot roll control loop including SAS and interconnect.

The assumed pilot describing function is

$$Y_P \approx K_{P_\varphi} \tag{6}$$

The roll and yaw feedback stability augmentation transfer functions including the high-pass washout filters are

$$Y_p = \frac{K_p s}{(s + \frac{1}{\tau_{wo}})} \tag{7}$$

$$Y_r = \frac{K_r s}{(s + \frac{1}{\tau_{wo}})} \tag{8}$$

The closed-loop transfer function (pilot, SAS, and vehicle) now becomes

$$Y_P\left(\frac{\varphi}{\delta_a}\right)' = \frac{K_{P_\varphi}(A_\varphi s^4 + B_\varphi s^3 + C_\varphi s^2 + D_\varphi s + E_\varphi)}{(As^6 + Bs^5 + Cs^4 + Ds^3 + Es^2 + Fs + G)} = \left(\frac{N_{\varphi/\delta_a}}{\Delta}\right)'$$

Figures 15(a) to 15(e) present the root loci for the specified conditions at constant angles of attack from 6° to -2°, in 2° increments. The zeros and poles for each of the angles of attack are tabulated in table 8. Figures 15(a) to 15(c) are similar, in that as the loop is closed the locus remains clear of the imaginary axis; however, the

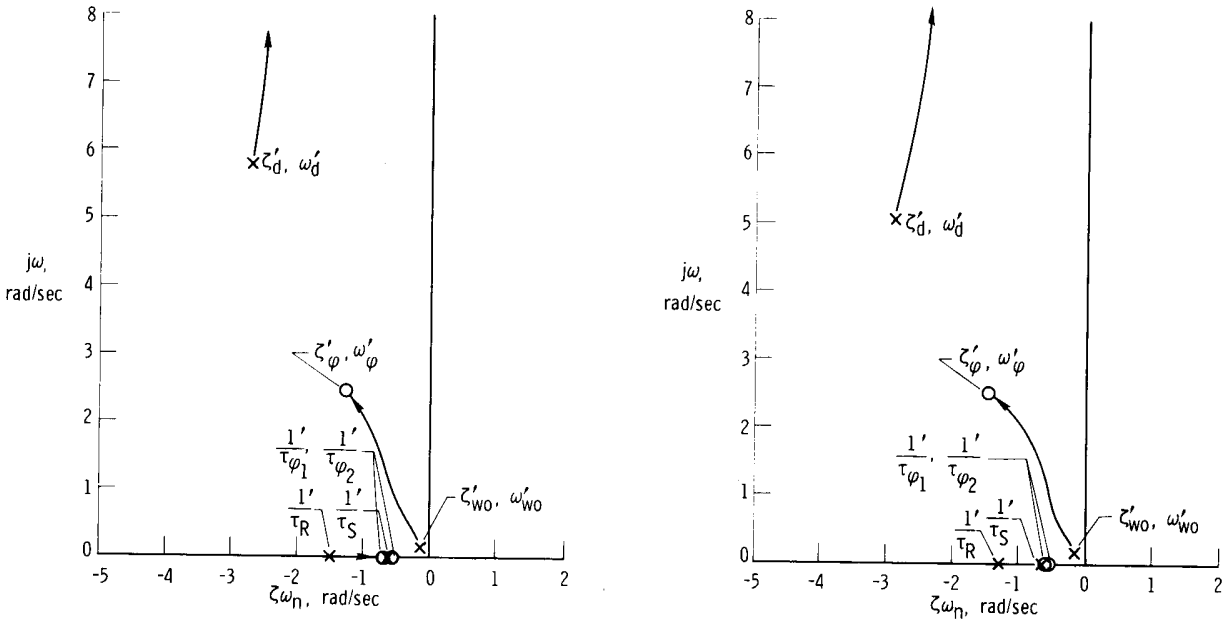

(a) $\alpha = 6^o$.

(b) $\alpha = 4^o$.

Figure 15. Complex plane plot of the root loci of the bank-angle-to-aileron transfer function with the SAS on, including roll and yaw washout filters, and assuming a pure gain pilot for the M2-F2. M = 0.48; V = 159.5 m/sec (523 ft/sec); q = 12,100 N/m^2(253 lb/ft^2); K_p = 0.2; K_r = 0.4; K_I = 0.45.

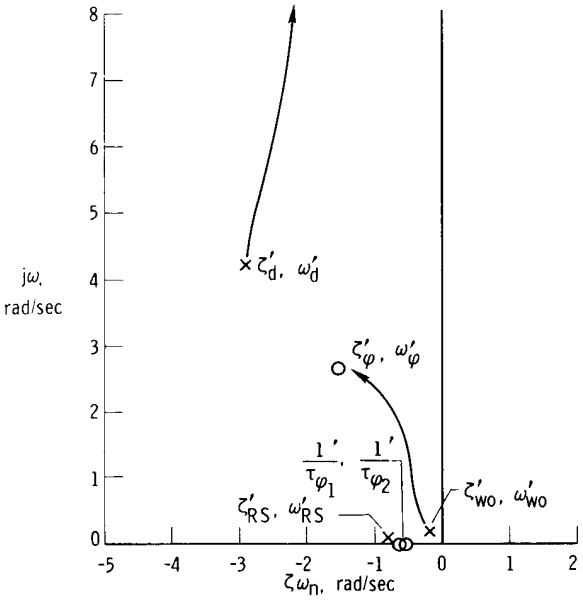

(c) a = 2°.

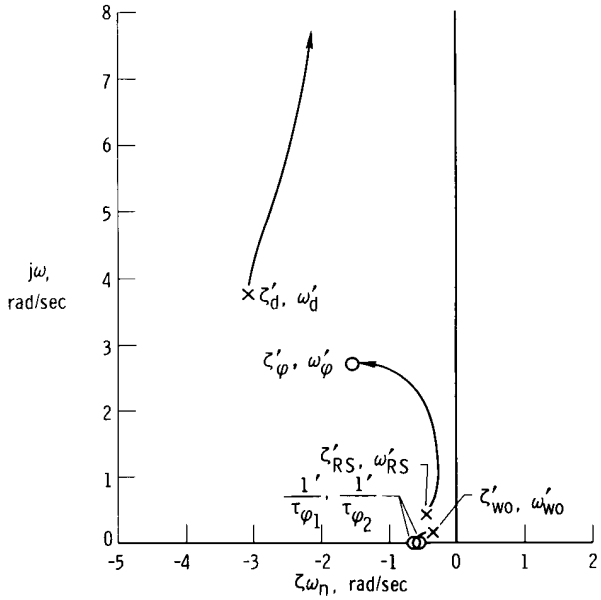

(d) a = 0°.

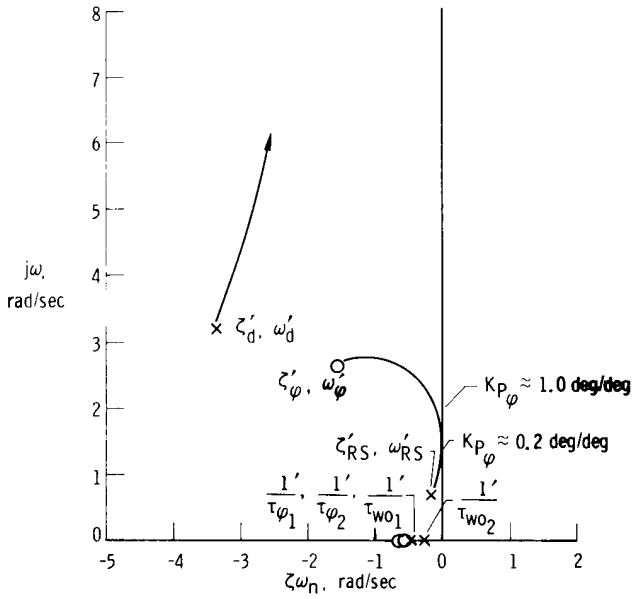

(e) a = -2°.

Figure 15. Concluded.

roll-mode pole migrates toward the imaginary axis and at 2° angle of attack the coupled roll-spiral mode appears. The bank-angle zero remains essentially stationary while the Dutch roll pole migrates in the direction of decreasing frequency. In figure 15(d) the roll-spiral mode has migrated up and to the right. The locus initially converges toward the imaginary axis and, as the gain is increased, it becomes parallel. At higher gains it moves away from the imaginary axis. At an angle of attack of -2° (fig. 15(e)), a lateral handling-qualities problem may be expected to develop in the form of a closed-loop PIO. From the figure it can be seen that the coupled roll-spiral-mode pole has continued its migration toward the imaginary axis and instability; the zero has remained stationary. As the bank angle is controlled in a pure gain fashion, the locus approaches the imaginary axis and a PIO. The gain required to approach the imaginary axis at its closest point ($\omega \approx 1.3$ rad/sec) is approximately 0.3° of aileron per degree of bank angle or 0.23 centimeter (0.09 inch) of lateral stick per degree of bank angle, which is a reasonable value. In this instance,

near-neutral closed-loop oscillations could be on the order of 1 rad/sec to 2 rad/sec with corresponding gains of approximately 0.2 deg/deg and 1.0 deg/deg, respectively.

The frequencies of in-flight pilot-induced oscillations are of interest. The PIO frequencies of figures 10 and 11 are on the order of 1.6 rad/sec and close to those predicted by the data of figure 15(e). The PIO frequency of figure 8 is approximately 2.7 rad/sec, which is higher than would be predicted by the data in figure 15(e). The interconnect ratio of this PIO was not constant and influenced the vehicle response significantly.

This systems analysis indicates that the M2-F2 vehicle could encounter closed-loop handling-qualities problems at -2° angle of attack at the flight conditions specified.

Simulator analysis. – To complement the theoretical analysis, a six-degree-of-freedom simulation of the M2-F2 vehicle was implemented. The lateral-directional aerodynamic characteristics used in this study are summarized in table 5. The pilot's cockpit control characteristics were similar to those of the flight vehicle. Instrument displays included a three-axis attitude indicator, which also displayed angle of sideslip on the vertical needle, and angle-of-attack, airspeed, altitude, and normal-acceleration indicators.

The pilot was requested to perform the following two tasks:

(1) Fly a nominal M2-F2 pattern from an altitude of approximately 6710 meters (22,000 feet) at an indicated airspeed of 190 knots and an initial pitch attitude of -10°. When roll out of the final turn was almost complete, push over to 300 knots and coordinate aileron input with rudder-pedal input.

(2) Repeat the task presented in item (1), except do not coordinate with rudder.

The first task was requested so that the simulator results could be compared with flight data. The second task was intended to illustrate the PIO problem without coordinated aileron and rudder control and to provide data for comparison with the systems analysis.

Figures 16(a) and 16(b) present the simulator time histories obtained from the two tasks. Figure 16(a), a time history of the first task, shows that as zero bank angle is approached the pilot attempts to arrest the change of bank angle and a PIO develops. After approximately one cycle, the pilot attempts to coordinate rudder with aileron; however, this drives the system more unstable. Recovery is rapid after use of rudder is discontinued, angle of attack is increased, and the large aileron commands are relaxed. The rate of change of the bank angle correlates with induced sideslip angle.

Figure 16(b) is a time history of the second task. Again, as zero bank angle is approached, angle of attack is decreased through zero. Zero bank angle is exceeded and the pilot attempts to return it to zero; again, an immediate PIO develops. Recovery is accomplished after aileron control is relaxed and angle of attack is increased.

The PIO frequencies of figures 16(a) and 16(b) are approximately 2.1 rad/sec and 1.3 rad/sec, respectively. These frequencies are close to those of the in-flight pilot-induced oscillations and the predictions of figure 15(e).

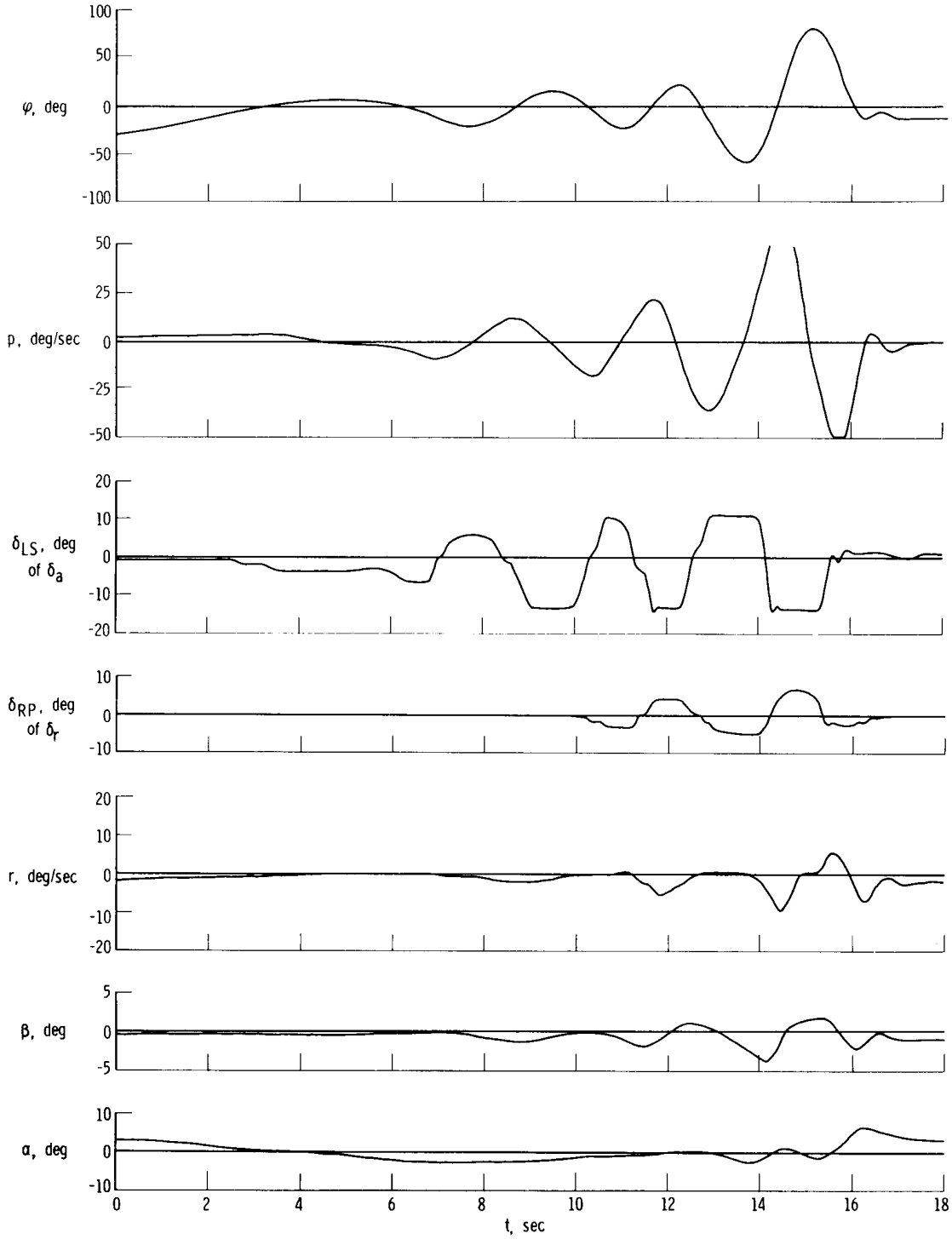

(a) Pilot coordination of aileron with rudder input.

Figure 16. M2-F2 six-degree-of-freedom simulator time history of final turn and approach to landing. $K_p = 0.2$; $K_r = 0.4$; $K_I = 0.45$.

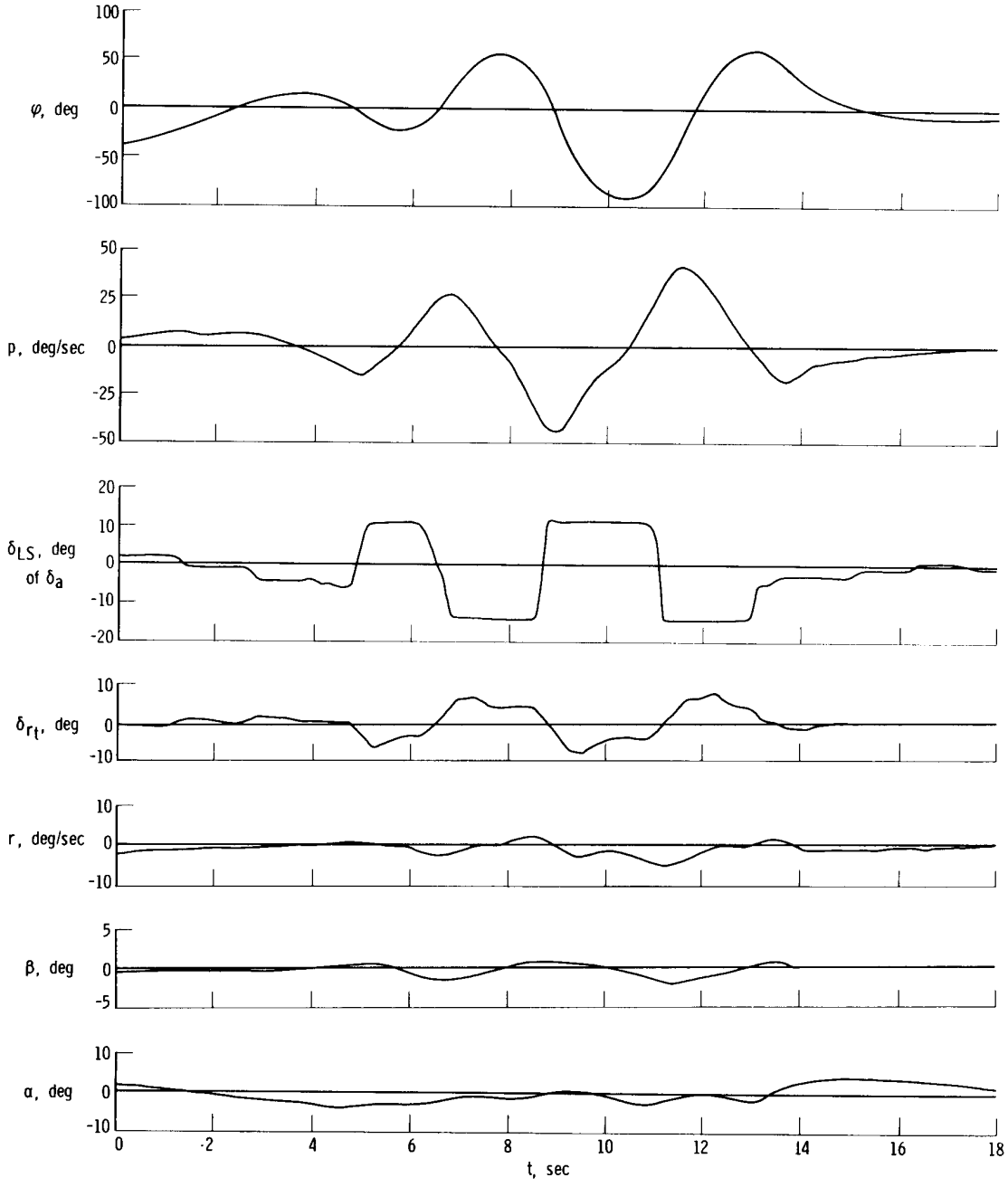

(b) Pilot lateral control with aileron only.

Figure 16. Concluded.

The pilot made the following comments concerning the simulated M2-F2 landing approach task:

"The lateral-directional instability became apparent on the pushover to the final approach. The ensuing roll oscillation was divergent using ailerons only and was aggravated by the use of rudders. Recovery was made by increasing alpha above 0°. At the low alpha (≈ -2.5°), the lateral-directional task received a pilot rating of 10.

"The simulation appeared to match the characteristics of the flight vehicle quite closely. It appeared that the simulation PIO was as easily induced as was the PIO in the flight vehicle."

It should be noted that the simulation evaluation pilot also experienced the PIO on the sixteenth flight of the M2-F2 vehicle.

Evaluation of flight, systems analysis, and simulator results. – The flight data showed a low-angle-of-attack, pilot-induced oscillation and the similarity of each of the three oscillations. The systems analysis showed a roll and spiral mode pole migration within the complex plane as angle of attack was varied. As these two poles converged, they formed the complex coupled roll-spiral-mode pole which migrated toward the imaginary axis and instability as a function of decreasing angle of attack. In physical terms, as the angle of attack was decreased, the roll axis would become less and less damped, or very "loose" as evaluated by the pilot. Depending on the extent of the excitation, the roll-spiral mode could appear to be a lateral trim problem; that is, if the pilot intended to fly "wings level," at relatively low gain, and the roll-spiral mode was excited in some way, he would not allow the bank angle to drift to any large error and, therefore, not observe the oscillatory characteristics of this mode. The pilot comments from flight 15 concerning lateral trim and "lateral-directional nibbling" at angles of attack of 5° and below are particularly interesting in view of the pilot rating of 6. As the roll-mode pole migrates to the right, the ailerons would still command roll rate; however, the time required to reach a given rate would become longer and longer, thus making the ailerons appear to the pilot to be more of an acceleration-ordering control over relatively short intervals of time.

One of the major conclusions of references 4 and 5 indicated that, even though the ailerons order bank angle (linear theory) for the coupled roll-spiral mode, the pilot may not be conscious of this because the mode may be slow to reach a steady state. Rather, he may see the ailerons as acceleration-, rate-, or position-ordering according to the amount of response he observes before he decides he should do something about the motion of the vehicle. Reference 4 pointed out that apparent acceleration-ordering ailerons could be acceptable for a reentry vehicle if large, rapid maneuvering was not required. When large, rapid bank-angle corrections were required, to correct for gusts, for example, acceleration-ordering roll control was objectionable.

On this basis, then, it may be inferred that, when acceleration-ordering ailerons are used to command a particular roll rate, aileron pulses would be required if the lateral axis were sufficiently lightly damped. Reference 1 indicates that this mode of aileron operation was utilized during an M2-F2 flight in which a 360° overhead approach to landing was used. Following this flight, the pilot reported that "without roll and yaw augmentation, bank-angle control was not as precise as desired, but turns could be made. The vehicle was susceptible to pilot-induced oscillations. Lateral stick pulses were effective in changing bank angle."

The simulator data also indicated that the lateral handling qualities of the M2-F2 vehicle were generally adequate until, at reduced angles of attack as the pilot controlled bank angle, a closed-loop PIO was generated.

The systems analysis results suggest that if the formation of the coupled roll-spiral mode could be precluded, or if the pole location of this mode could be altered to a more favorable position within the complex plane, the handling qualities at low angles of attack would be improved.

In general, the results of both the systems analysis and the simulator study are in good agreement with the conclusions of references 4, 5, and 6.

Factors Influencing Zero-Pole Locations of the M2-F2 Vehicle

Poles. – The nature of the poles is determined by the transfer-function-denominator characteristic equation of the basic vehicle when equated to zero. When the roll and spiral modes are coupled, this expression is

$$\Delta = As^4 + Bs^3 + Cs^2 + Ds + E = (s^2 + 2\zeta_{RS}\omega_{RS}s + \omega_{RS}^2)(s^2 + 2\zeta_d\omega_d s + \omega_d^2) \qquad (10)$$

Table 6 shows that, as the angle of attack is decreased, the A, B, and E coefficients remain relatively constant while the C and D coefficients vary over a wide range. The C coefficient can be related to the Dutch roll frequency by the approximation

$$C \approx \omega_d^2 \approx N_\beta - L_\beta\left(\alpha - \frac{I_{XZ}}{I_Z}\right) \qquad (11)$$

Variations of this coefficient affect the position of the Dutch roll mode pole parallel to the imaginary axis (fig. 12). The D coefficient, however, changes from positive to negative as angle of attack is decreased, and from Descartes' rule of signs (ref. 13) it is known that, with two variations in sign by the coefficients, at least one and at the most two poles will be in the right-hand plane when this occurs. The D coefficient may be approximated by

$$D = 2\zeta_d\omega_d\omega_{RS}^2 + 2\zeta_{RS}\omega_{RS}\omega_d^2 \approx \alpha(L_\beta N_r - N_\beta L_r) + \left[L_\beta\left(N_p - \frac{g}{V}\right) - N_\beta L_p\right] \qquad (12)$$

Reference 7 presents an extensive mathematical analysis of the role of the lateral-directional transfer-function denominator in determining the existence of roll-spiral coupling when the coefficients meet specific criteria. Also discussed is the influence of important aerodynamic parameters involved in producing this coupling. Tables 6 and 7 show that the migration of the roll, spiral, and coupled roll-spiral poles is highly dependent on the magnitude as well as the sign of the D coefficient (positive desired). From the approximate equation for this coefficient (eq. (12)), it can be seen that the dominant parameters are α, $L_\beta N_r$, $L_\beta\left(N_p - \frac{g}{V}\right)$, and $N_\beta L_p$. If, then, the more important parameters of this coefficient can be controlled, the possibility of providing

acceptable pole locations should be enhanced. Certain implicit limitations will not be considered in the following analysis: (1) the requirement to operate in the -2° angle-of-attack region; (2) an increase in roll damping alone through roll SAS gain, even though theoretically the roll-spiral-mode characteristics can be improved in this manner. The primary reason for not considering the second limitation is that the M2-F2 vehicle was restricted to operation at lower roll SAS gains because of practical control system considerations. Further, the divergences of figures 8, 10, and 11 occurred at $K_p = 0.6$, 0.4, and 0.2, respectively, and the PIO was not precluded at twice or three times the gain of the PIO of figure 11. The possibility of improving the roll-spiral-mode characteristics by judiciously selecting a combination of roll SAS gain and interconnect ratio, which affects both poles and zeros, is discussed later. In the following discussion three possibilities that affect only the poles are considered:

(1) Reducing the very high effective dihedral by changing the configuration or providing a β feedback to the ailerons.

(2) Providing a feedback signal to the rudder proportional to roll rate, that is, making N_p more negative thus reducing the strong effect of $L_\beta(N_p - \frac{g}{V})$.

(3) Improving the control characteristics so that acceptable pole and zero locations can be attained through the existing roll and yaw rate feedback loops.

The problem of very high effective dihedral, L_β, is not unique to the M2-F2 vehicle but is a general characteristic of lifting body configurations. A configuration change of sufficient magnitude to appreciably reduce the effective dihedral would not be practical. A β feedback could be implemented; however, from practical considerations such a signal is difficult to work with because of its susceptibility to gust disturbances and boom-vane dynamics. Further, the gain requirements of a β feedback to effectively reduce the effective dihedral would be unrealistically high. Therefore, a β feedback was not implemented.

The yawing moment due to roll rate, N_p, is of particular interest because of its strong influence on vehicle lateral-directional response characteristics and resultant influence on handling qualities through the parameter $L_\beta(N_p - \frac{g}{V})$. Reference 14 presents the results of an analysis of handling-qualities problems associated with this parameter because of its influence on transfer-function factors and associated response time histories. Figures 17(a) and 17(b) illustrate the effects on the transfer-function poles as a function of C_{n_p} for the -2° angle-of-attack condition. The transfer-function-denominator coefficients, poles, and response characteristics are presented in table 9. From figure 17 it can be seen that as C_{n_p} is varied from 0.30 to -0.75, the Dutch roll, coupled roll-spiral mode, and ultimately the roll and spiral poles are drastically affected, as is the D coefficient. As the coupled roll-spiral mode is stabilized, with decreased C_{n_p}, the Dutch roll mode is destabilized. This would suggest that an appropriate signal proportional to roll rate could be transmitted to the rudders, thereby generating a more favorable yawing moment as a function of roll rate and opposing the natural N_p characteristics of the vehicle.

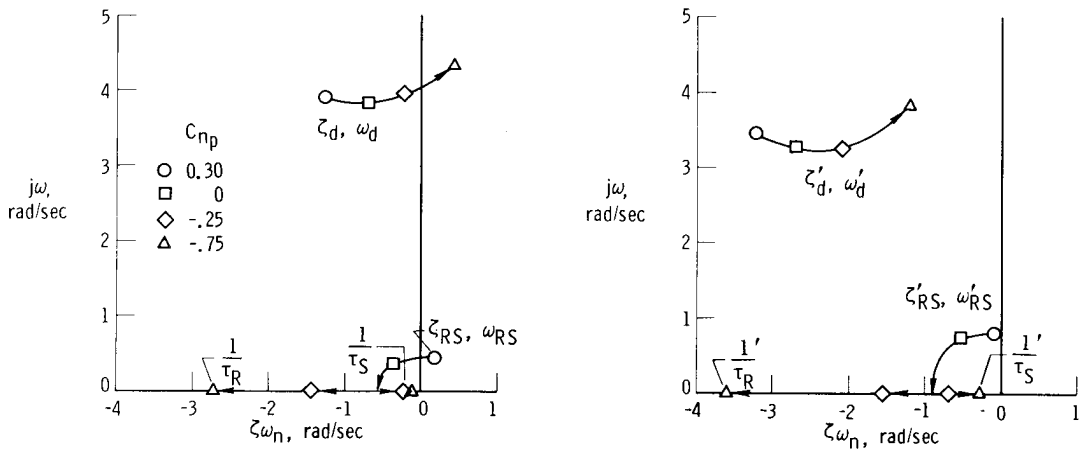

(a) Variation with $K_p = K_r = 0$. *(b) Variation with $K_p = 0.2$ and $K_r = 0.4$.*

Figure 17. Complex plane plot of the open-loop M2-F2 lateral-directional poles as a function of yawing moment due to roll rate. M = 0.48; V = 159.5 m/sec (523 ft/sec); q = 12,100 N/m^2 (253 lb/ft^2); $\alpha = -2^0$; $K_I = 0.45$.

A system of this type, which would appear to offer a reasonable solution to the problem of the poor coupled roll-spiral pole locations, was considered for the M2-F2 vehicle; however, because of limited and questionable aerodynamic data and potential hazards in other flight regions, it was not implemented. In the mechanization of the M2-F2 interconnect, a yawing moment proportional to roll rate was generated by means of the roll SAS and interconnect, as can be seen in figure 14.

Zeros. – In the analysis of item 3 (page 33) it is necessary to consider the control characteristics, which imply transfer-function zeros, and their effect on pole location through the feedback loops. Handling-qualities investigators have frequently attempted to present lateral-directional handling-qualities requirements based on the ratio $\frac{\omega_\varphi}{\omega_d}$ which indicates only the relative distance apart of the bank-angle zero and Dutch roll mode pole along the imaginary axis and does not adequately describe the lateral handling-qualities situation, as pointed out in references 2 and 15. References 14 and 15 determined acceptable bank-angle-zero locations for a variety of Dutch roll, roll, and spiral poles. In the final analysis it is the degree of interaction of all the important lateral-directional zeros and poles which determines the degree of acceptability of the handling-qualities characteristics, including roll-spiral poles, if this mode exists.

As previously discussed, the M2-F2 yawing moment due to aileron deflection was adverse, necessitating an aileron-to-rudder interconnect. It was shown in figure 12 and table 7 that with $K_I = 0$ the bank-angle transfer-function numerator yielded two real zeros (eq. (4)). This, in terms of handling qualities, represents a situation in which roll control by the ailerons is negated by induced sideslip angle, β, and roll reversal occurs. With $K_I = 0.45$ the bank-angle zeros are complex and migrate into the left-hand plane. The second-order transfer-function-numerator parameter, $\omega_\varphi{}^2$, is the dominant term in the discriminant of this quadratic factor and, therefore, exerts

a dominant influence on the nature of the zeros. This parameter may be approximated by

$$\omega_\varphi{}^2 = \frac{C_\varphi}{A_\varphi} \approx N_\beta - L_\beta \frac{N_{\delta_a}}{L_{\delta_a}} \tag{13}$$

From this expression the effect of adverse aileron yaw in conjunction with very high effective dihedral is apparent; that is, the ratio of $\frac{N_{\delta_a}}{L_{\delta_a}}$ can remain relatively small but still exert considerable influence on both the sign and magnitude of $\omega_\varphi{}^2$. For the M2-F2 vehicle, $|L_\beta| \approx 13|N_\beta|$ and the ratio of $\frac{N_{\delta_a}}{L_{\delta_a}}$, when $K_I = 0$, is approximately -0.17, making $\omega_\varphi{}^2 \approx -1.2\,N_\beta$ and resulting in real zeros of approximately ±3. (See tables 6 and 7.)

The effect of the interconnect can now be illustrated for the idealized situation, with no system lags or nonlinearities. When the aileron commands a proportional rudder input, an apparent or quasi-aileron yaw is generated. The effective aileron yawing moment and rolling moment generated in this manner can be expressed as

$$\left(N_{\delta_a}\right)_{eff} = N_{\delta_a} - K_I N_{\delta_r} \tag{14}$$

and

$$\left(L_{\delta_a}\right)_{eff} = L_{\delta_a} - K_I L_{\delta_r} \tag{15}$$

Thus, the aileron-to-rudder interconnect makes $\left(N_{\delta_a}\right)_{eff}$ more positive and $\left(L_{\delta_a}\right)_{eff}$ more negative, resulting in a more favorable ratio of $\frac{\left(N_{\delta_a}\right)_{eff}}{\left(L_{\delta_a}\right)_{eff}}$, in this instance, where $K_I = 0.45$, of approximately 0.016 (table 6). With this ratio, $\frac{\left(N_{\delta_a}\right)_{eff}}{\left(L_{\delta_a}\right)_{eff}}$, $\omega_\varphi{}^2 \approx 1.2\,N_\beta$, resulting in imaginary zeros and ω_φ on the order of 3.

The interconnect of the M2-F2 vehicle was designed so that every aileron deflection produced a proportional rudder deflection, depending on the setting of the manually operated ratio changer. The aileron response to roll-rate SAS therefore actuated the rudders proportional to roll SAS gain and interconnect setting. This not only affected bank-angle-zero location but the location of the poles as well (fig. 14). The rationale of the M2-F2 interconnect design, which should not be considered necessarily optimum, is beyond the scope of this report.

The augmented or total rolling moment due to roll rate can be expressed as

$$L_{p_t} = L_p - K_p\left(L_{\delta_a}\right)_{eff} = L_p - K_p\left(L_{\delta_a} - K_I L_{\delta_r}\right) \tag{16}$$

which results in a net increase, negatively, of the rolling moment resisting roll rate, the desired effect. Similarly, the yawing moment due to roll rate is altered by

$$N_{p_t} = N_p - K_p\left(N_{\delta_a}\right)_{eff} = N_p - K_p\left(N_{\delta_a} - K_I N_{\delta_r}\right) \tag{17}$$

From this expression, it can be seen that the net effect on the yawing moment due to roll rate depends largely on the effective aileron yaw. Thus, to provide an apparent favorable ratio of $\frac{N_{\delta_a}}{L_{\delta_a}}$, other important control and damping characteristics were compromised, such as total roll control, augmented roll damping, and yaw due to roll rate. Some of the results of reference 15, in which the in-flight lateral-directional handling qualities for a variety of vehicle dynamics were investigated, are of interest. Emphasis in this study was placed on determining acceptable locations for the bank-angle zero with respect to the Dutch roll, roll, and spiral poles as well as $\left|\frac{\varphi}{\beta}\right|_d$ ratios. This study concluded that zeros to the left of the Dutch roll pole were generally better than those to the right and that these configurations showed less deterioration in pilot ratings as the zero was displaced from its optimum location by variations in the $\frac{N_{\delta_a}}{L_{\delta_a}}$ ratio. It was also concluded that the best $\frac{N_{\delta_a}}{L_{\delta_a}}$ ratio was primarily a function of the yawing moment due to roll rate, N_p.

It is now apparent that in conjunction with the very high effective dihedral the closed-loop handling qualities of the M2-F2 vehicle were sensitive to combinations of roll SAS gain and interconnect-ratio setting. With judicious selection of both roll SAS gain and interconnect ratio over the Mach number—angle-of-attack envelope, acceptable zero-pole relationships may have been possible. However, after the landing accident it was decided that making a simple aerodynamic modification to improve the lateral handling characteristics would be preferable to relying on the control system. Wind-tunnel results had indicated that the aileron yawing characteristics of the vehicle could be made favorable with the addition of a center fin, which would introduce the possibility that the interconnect could be eliminated or that the required gain setting could be greatly reduced. Thus it appeared that a relatively simple airframe modification would greatly improve the lateral stability and handling qualities.

M2-F3 Lateral Controllability

Airframe modification. – The M2-F2 vehicle was rebuilt, modified to incorporate a fixed center fin (fig. 4), and designated the M2-F3. Wind-tunnel tests indicated that the effective dihedral, aileron effectiveness, and directional-stability derivatives were relatively unchanged. There was a slight increase in drag, but the aileron

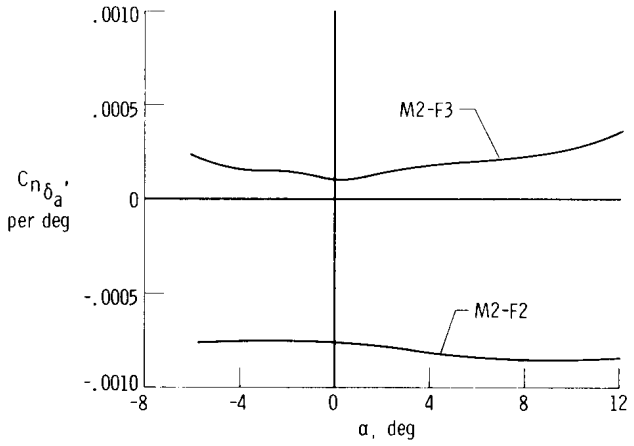

Figure 18. Aileron yawing-moment characteristics of the M2-F2 and M2-F3 at M = 0.5 predicted from small-scale wind-tunnel results.

yawing-moment characteristics were predicted to be favorable (fig. 18). This effect was attributed to the addition of the center-fin area upon which the pressure generated by the upper flaps operates counter to that of the inside of the outboard fins, thus providing favorable aileron yawing-moment characteristics.

Systems analysis. – With favorable aileron yawing-moment characteristics, the ratio of $\frac{N_{\delta_a}}{L_{\delta_a}}$ would be positive without the aileron-to-rudder interconnect. The bank-angle transfer-function zeros, therefore, could be expected to be complex without the aid of the interconnect. Preliminary simulator results indicated that an interconnect and a roll washout filter would not be required in the glide flight region. Therefore, these items are not considered in the following analysis.

The M2-F3 dimensionalized aerodynamic derivatives, coefficients of the bank-angle transfer function, zeros, poles, and response characteristics are presented in table 10. To compute the dimensional aileron yawing derivatives, only the aileron yawing-moment coefficients (fig. 18) were changed; the other aerodynamic and inertia characteristics, as well as the other stability and control derivatives and the moments of inertia, were the same as those of the M2-F2 vehicle. Figure 19 presents the complex plane plot of the augmented M2-F3 vehicle at the flight conditions of figure 11; yaw washout was not considered. A comparison of the M2-F3 zeros and poles of figure 19 with the M2-F2 zeros and poles of figure 13 shows that the Dutch roll poles are similar. The zeros are now complex without the aid of the interconnect. The roll-mode pole appears to have been significantly improved. The coupled roll-spiral mode does not exist until approximately 2° angle of attack is reached, as compared with approximately 5° for the M2-F2 vehicle. Figures 20(a) to 20(e) present the root loci at constant angles of attack for the bank-angle transfer function, assuming a pure gain pilot and including yaw washout (table 11). The formation of the coupled roll-spiral

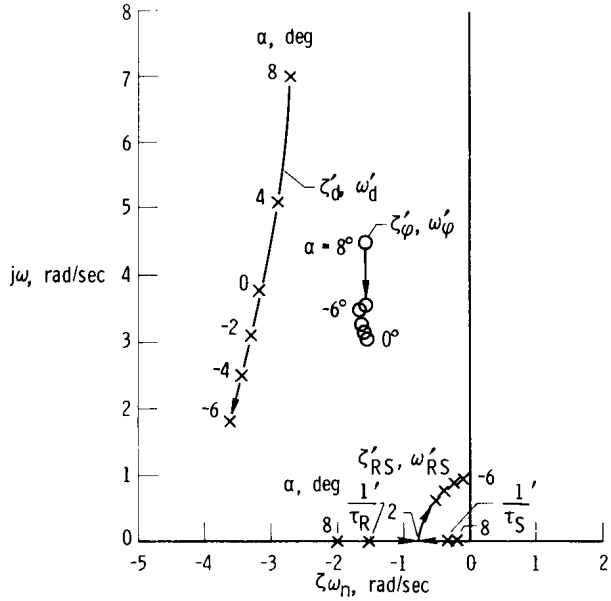

Figure 19. Complex plane plot of the SAS-on open-loop bank-angle-to-aileron transfer-function zeros and poles as a function of angle of attack for the M2-F3 at $K_I = 0$. $M = 0.48$; $V = 159.5$ m/sec (523 ft/sec); $q = 12{,}100$ N/m^2 (253 lb/ft^2); $K_p = 0.2$; $K_r = 0.4$.

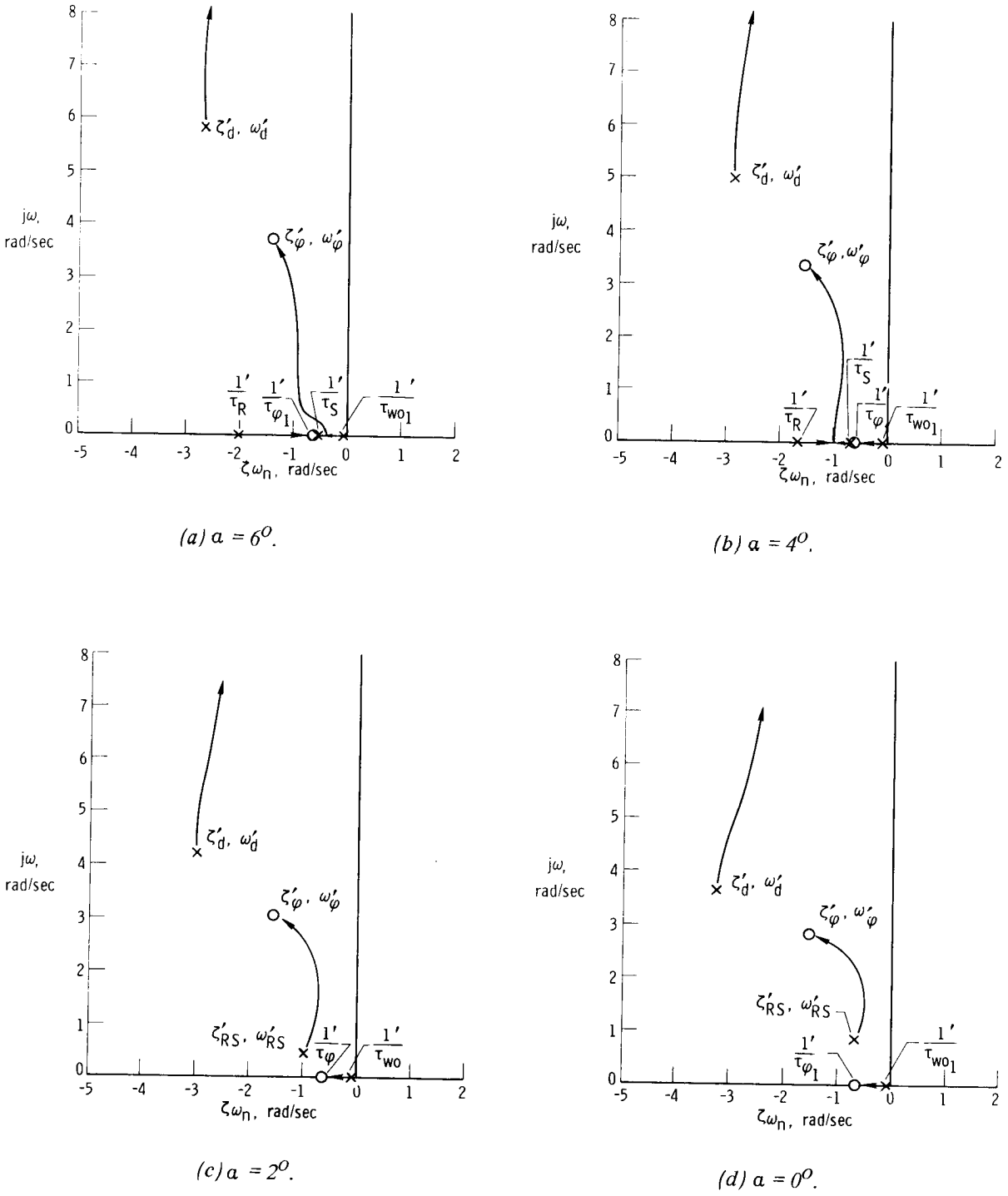

(a) $a = 6^o$.

(b) $a = 4^o$.

(c) $a = 2^o$.

(d) $a = 0^o$.

Figure 20. Complex plane plot of the root loci of the bank-angle-to-aileron transfer function with SAS on, including yaw washout filter, and assuming a pure gain pilot. M = 0.48; V = 159.5 m/sec (523 ft/sec); q = 12,100 N/m^2 (253 lb/ft^2); $K_p = 0.2$; $K_r = 0.4$.

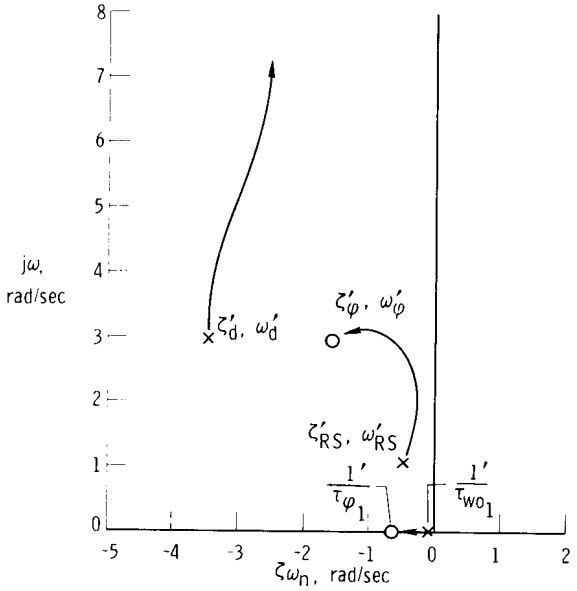

(e) $\alpha = -2^o$.

Figure 20. Concluded.

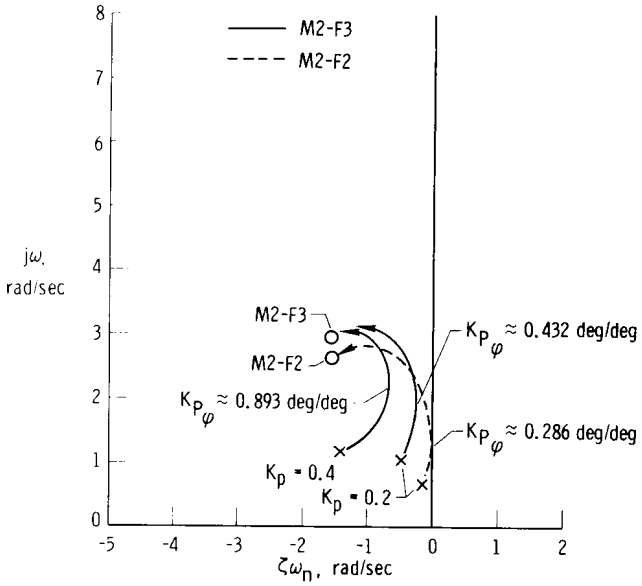

Figure 21. Comparison of M2-F2 and M2-F3 roll spiral at $\alpha = -2^o$ and for several roll SAS gains. M = 0.48; V = 159.5 m/sec (523 ft/sec); q = 12,100 N/m^2 (253 lb/ft^2); $K_r = 0.4$; $K_I = 0.45$ (M2-F2 only).

mode was delayed until an angle of attack between 2° and 4° was reached (compared with approximately 5° for the M2-F2 vehicle), and at the -2° condition the root loci close toward the imaginary axis; however, they do not become tangent to the imaginary axis or cross into the unstable region. The M2-F3 vehicle at the -2° angle-of-attack flight condition should be less sensitive to pilot-induced oscillations than the M2-F2 vehicle; however, the tendency is still present.

Figure 21 summarizes and compares the M2-F2 and M2-F3 roll-spiral pole and bank-angle-zero loci at $\alpha = -2°$ for $K_p = 0.2$ and $K_r = 0.4$, and for the M2-F3 vehicle at $K_p = 0.4$. The roll-damping-gain increase significantly shifts the coupled roll-spiral pole to the left; in addition, the gain required to approach the imaginary axis at its closest point is more than double that for $K_p = 0.2$. It would be expected, therefore, that higher roll SAS gain would also significantly lessen the M2-F3 PIO tendencies in this flight region.

Simulator analysis. – To complete the analysis of the M2-F3 vehicle, a six-degree-of-freedom simulation was generated. As in the systems analysis, the only aerodynamic derivative change was in the aileron yawing-moment characteristics. The aileron-to-rudder-interconnect-ratio setting was reduced to zero, and the pilot's aileron authority was increased to ±20°.

The task presented to the pilot was, as with the M2-F2 vehicle, to fly a nominal M-2 approach pattern from approximately 6710 meters (22,000 feet) altitude and at approximately 190 knots indicated airspeed. Figure 22 presents the M2-F3 simulator time history of the final turn and approach to landing with $K_p = 0.2$ and $K_r = 0.4$.

As the roll out of the turn was completed, the pilot pushed over to -4° angle of attack; however, control was not lost and a PIO was not generated even though the pilot

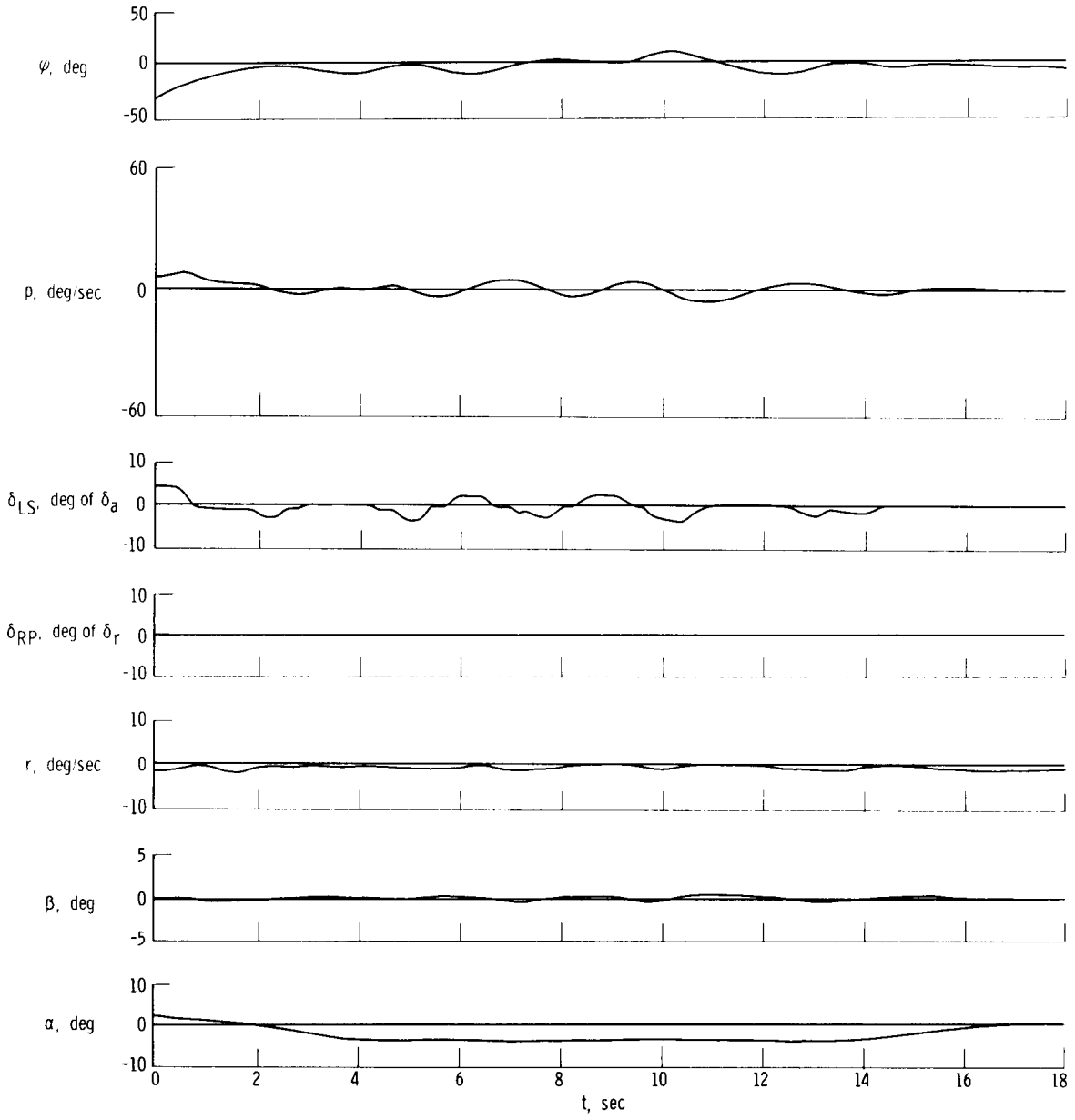

Figure 22. M2-F3 six-degree-of-freedom simulator time history of final turn and approach to landing with no pilot rudder input. $K_p = 0.2$; $K_r = 0.4$.

continued to roll the vehicle through bank angles of ±5° to ±10°. Induced angle of sideslip was minimized because $C_{n\delta_a}$ was slightly positive, obviating rudder inputs through the interconnect.

The second task presented to the pilot was to repeat the same flight profile except to turn both roll and yaw SAS off. Figure 23 presents the simulator time history of this maneuver. As rollout was accomplished, the angle of attack was reduced through zero. The pilot again controlled bank angle, this time through approximately ±20°. A divergence was not experienced until aileron was coordinated with a slight amount of rudder at approximately -4° angle of attack.

The pilot made the following comments concerning the simulated M2-F3 landing approach task:

"Again the task specified was to fly that portion of an M2-F2 flight from the presented initial conditions through the final turn, approach, flare, and landing. At low alpha (-2°) no lateral-directional instability presented itself. The vehicle could be controlled using ailerons only; however, use of ailerons and rudders caused a divergent PIO.

"With the roll and yaw dampers off, the vehicle could be flown normally if the angle of attack was not lowered below approximately -2°. The vehicle could be flown down to -4° alpha using ailerons only; however, the use of rudders in this area caused divergent lateral-directional oscillations. At -2° alpha, pilot ratings of 5 were given."

Flight.– Results from the first two flights of the M2-F3 vehicle generally substantiated the more favorable roll control characteristics predicted from wind-tunnel data and the improved lateral handling qualities determined in the analytical and simulator studies compared with the results for the M2-F2. Pilot ratings from flight, based on a modified Cooper scale (table 4), indicated excellent roll control characteristics with good lateral vehicle response. Ratings for lateral tasks ranged from 2.0 to 1.5. Figure 24, a time history of an M2-F2 and M2-F3 turn to final approach, shows that the M2-F2 pilot-induced-oscillation tendencies in the preflare landing were eliminated in the M2-F3. The M2-F2 vehicle rolled out of the left bank to a right bank as an S-turn maneuver was performed for energy management purposes. The general poor quality of the bank-angle modulation and high pilot stick activity were typical of the M2-F2 vehicle; however, the M2-F3 bank-angle control was precise and the pilot stick activity was minimal. It should be noted that in the M2-F3 vehicle the pilot's aileron authority was increased to ±20°.

Preliminary estimates of the lateral-directional derivatives from flight appear to generally confirm wind-tunnel predictions. The aileron control characteristics were generally substantiated, particularly the favorable yawing-moment characteristics presented in figure 18.

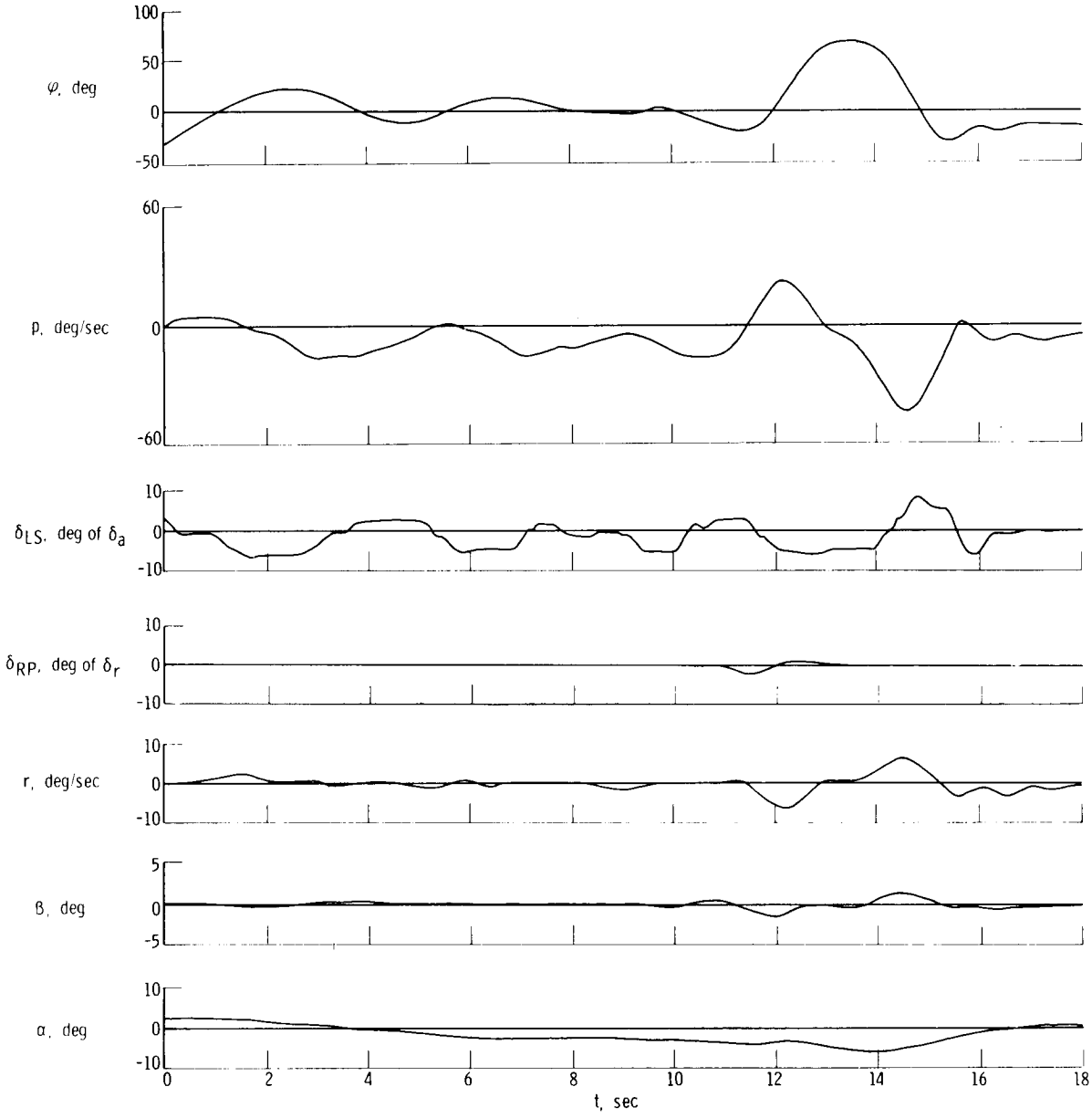

Figure 23. M2-F3 six-degree-of-freedom simulator time history of final turn and approach to landing with SAS off.

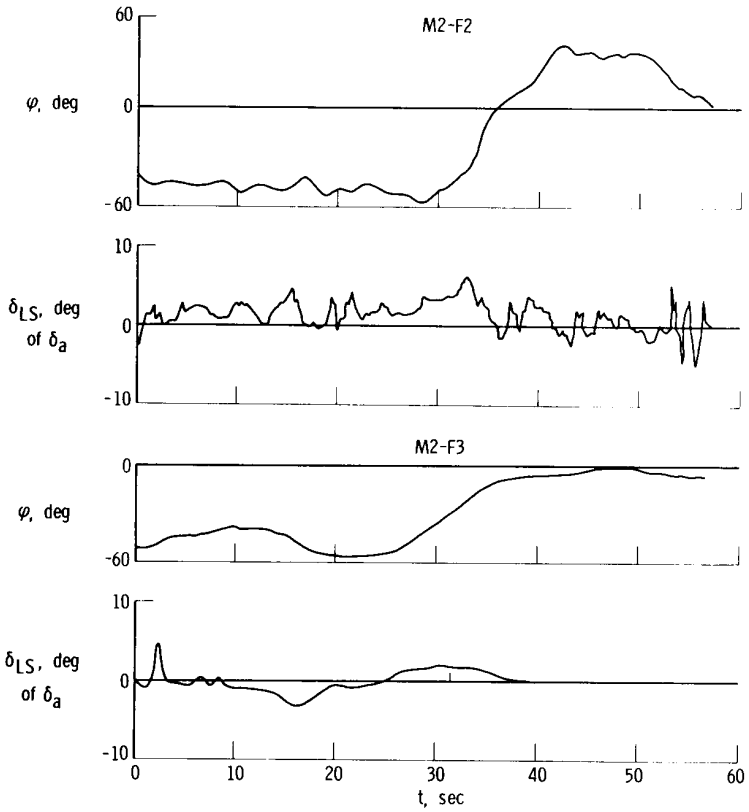

Figure 24. Comparison of lateral control and response in turn to final approach of M2-F2 and M2-F3. M2-F2: $K_p = 0.4$, $K_r = 0.6$, and $K_I = 0.49$; M2-F3: $K_p = 0.4$, $K_r = 0.4$.

CONCLUDING REMARKS

Severe lateral divergent oscillations were experienced during the 16 glide flights of the M2-F2 lifting body flight-research program. Operational requirements of the vehicle necessitated flight in the near-zero and below angle-of-attack flight region in the preflare situation. Control in this flight region was critical because of the strong lateral pilot-induced-oscillation (PIO) tendencies which were not precluded by normal operation of the flight control and stability augmentation systems. Each of the four program pilots was critical of the lateral handling qualities of the vehicle in this flight region; three of the pilots experienced severe lateral pilot-induced oscillations. Each oscillation subsided when the control technique was changed or angle of attack was increased, or both. Coordinated use of rudders aggravated the instability.

A systems analysis with the pilot in the loop related the preflare low-angle-of-attack lateral PIO tendencies to the formation of a coupled roll-spiral mode which caused the pilots to generate a closed-loop lateral instability. The coupled roll-spiral-mode characteristics were a strong function of angle of attack; that is, this mode became less stable at the lower angles of attack and, as a result, recovery could be accomplished by increasing angle of attack and changing control manipulation. A six-degree-of-freedom simulation of the M2-F2 vehicle generally verified that strong PIO

tendencies existed in the low-angle-of-attack preflare flight region and generally supported the flight data and analysis.

Generally, the formation of the M2-F2 coupled roll-spiral mode was attributed to the large effective dihedral characteristics in conjunction with a large positive yawing moment due to roll rate and operation in the negative angle-of-attack region. Contributing factors were the low natural roll damping and generally poor aileron control characteristics, particularly the very large adverse yawing moment due to aileron deflection.

Wind-tunnel data indicated that, with the addition of a fixed center fin, the yawing moment due to aileron deflection would become favorable without affecting other aerodynamic characteristics. Systems analysis and simulator studies indicated that the modified vehicle, designated the M2-F3, would not require an aileron-to-rudder interconnect in the normal glide flight region and would have improved lateral handling qualities in the low-angle-of-attack, preflare, landing-approach situation. The predicted improved lateral handling qualities resulted from improved aileron yawing-moment characteristics that eliminated the need for the aileron-to-rudder interconnect. Therefore, generally more favorable zero-pole combinations resulted.

Flight tests of the M2-F3 vehicle corroborated the systems analysis and simulator results. Pilot evaluation indicated excellent roll control and good vehicle response. No tendency toward lateral PIO was observed.

In general, the results of this study agree with other published flight and simulator results concerning roll-spiral coupling.

Flight Research Center,
National Aeronautics and Space Administration,
Edwards, Calif., April 16, 1971.

APPENDIX A

LATERAL-DIRECTIONAL EQUATIONS OF MOTION AND BANK-ANGLE TRANSFER FUNCTION

The side-force, rolling-moment, and yawing-moment equations were derived on the basis of a right-hand orthogonal body-axis system for a rigid airframe (fig. 25).

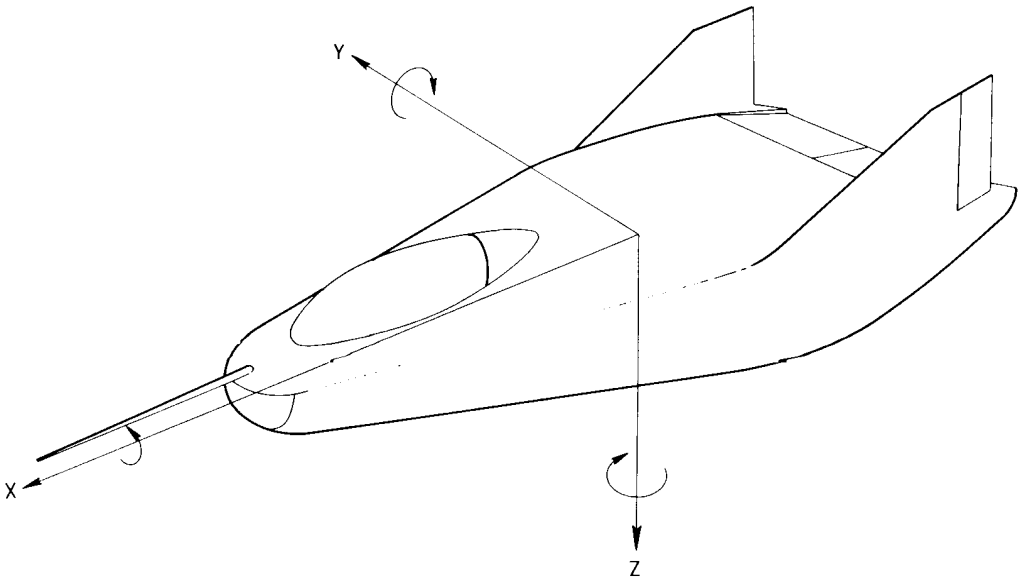

Figure 25. Right-hand axis system showing positive directions for all vector quantities, such as forces, moments, and accelerations.

The three equations in conventional dimensional form are as follows:

Side-force

$$\dot{\beta} = p\alpha - r + \frac{g}{V}\varphi + Y_{\beta}\beta + Y_{\delta_a}\delta_a + Y_{\delta_r}\delta_r$$

Rolling moment

$$\dot{p} = \frac{I_{XZ}}{I_X}\dot{r} + L_{\beta}\beta + L_p p + L_r r + L_{\delta_a}\delta_a + L_{\delta_r}\delta_r$$

Yawing moment

$$\dot{r} = \frac{I_{XZ}}{I_Z}\dot{p} + N_{\beta}\beta + N_p p + N_r r + N_{\delta_a}\delta_a + N_{\delta_r}\delta_r$$

APPENDIX A

In terms of the Laplace transform variable, s, this set of equations in matrix form is

$$\begin{bmatrix} (s - Y_\beta) - (s\alpha + \frac{g}{V}) & 1 & \\ - L_\beta & s(s - L_p) & -\left(\frac{I_{XZ}}{I_X}s + L_r\right) \\ - N_\beta & -s\left(\frac{I_{XZ}}{I_Z}s + N_p\right) & (s - N_r) \end{bmatrix} \begin{bmatrix} \beta \\ \varphi \\ r \end{bmatrix} = \begin{bmatrix} Y_{\delta_a} \\ L_{\delta_a} \\ N_{\delta_a} \end{bmatrix} \left[\delta_a\right]$$

from which the transfer function denominator is

$$\Delta = As^4 + Bs^3 + Cs^2 + Ds + E$$

The coefficients of the denominator are

$$A = \left(1 - \frac{I_{XZ}^2}{I_X I_Z}\right)$$

$$B = \left[-\left(L_p + N_r\right) + Y_\beta\left(\frac{I_{XZ}^2}{I_X I_Z} - 1\right) - I_{XZ}\left(\frac{L_r}{I_Z} + \frac{N_p}{I_X}\right)\right]$$

$$C = \left[N_\beta\left(1 - \frac{I_{XZ}}{I_X}\alpha\right) + L_\beta\left(\frac{I_{XZ}}{I_Z} - \alpha\right) - N_p L_r + L_p Y_\beta + N_r Y_\beta + L_r Y_\beta \frac{I_{XZ}}{I_Z} + N_p Y_\beta \frac{I_{XZ}}{I_X} + L_p N_r\right]$$

$$D = \left[\alpha\left(L_\beta N_r - N_\beta L_r\right) + \left(L_\beta N_p - N_\beta L_p - N_\beta \frac{I_{XZ}}{I_X}\frac{g}{V} - L_\beta \frac{g}{V}\right) + Y_\beta\left(N_p L_r - L_p N_r\right)\right]$$

$$E = \left(L_\beta N_r - N_\beta L_r\right)\frac{g}{V}$$

or, as expressed in terms of modal response characteristics,

Coefficient	Dutch roll and coupled roll spiral	Dutch roll, roll, and spiral
A	≈ 1.0	≈ 1.0
B	$2\zeta_d\omega_d + 2\zeta_{RS}\omega_{RS}$	$2\zeta_d\omega_d + \left(\frac{1}{\tau_R} + \frac{1}{\tau_S}\right)$
C	$\omega_d^2 + 4\zeta_d\zeta_{RS}\omega_d\omega_{RS} + \omega_{RS}^2$	$\omega_d^2 + 2\zeta_d\omega_d\left(\frac{1}{\tau_R} + \frac{1}{\tau_S}\right) + \frac{1}{\tau_R\tau_S}$
D	$2\zeta_d\omega_d\omega_{RS}^2 + 2\zeta_{RS}\omega_{RS}\omega_d^2$	$2\zeta_d\omega_d\left(\frac{1}{\tau_R\tau_S}\right) + \omega_d^2\left(\frac{1}{\tau_R} + \frac{1}{\tau_S}\right)$
E	$\omega_d^2\omega_{RS}^2$	$\omega_d^2\left(\frac{1}{\tau_R\tau_S}\right)$

APPENDIX A

The bank-angle transfer-function numerator is

$$A_\varphi = L_{\delta_a} + N_{\delta_a}\frac{I_{XZ}}{I_X}$$

$$B_\varphi = -L_{\delta_a}\left(N_r + Y_\beta\right) + N_{\delta_a}\left(L_r - \frac{I_{XZ}}{I_X}Y_\beta\right) + Y_{\delta_a}\left(L_\beta + \frac{I_{XZ}}{I_X}N_\beta\right)$$

$$C_\varphi = L_{\delta_a}\left(N_\beta + Y_\beta N_r\right) - N_{\delta_a}\left(L_\beta + Y_\beta L_r\right) + Y_{\delta_a}\left(N_\beta L_r - L_\beta N_r\right)$$

or

Coefficient	Real zeros	Complex zeros
A_φ	K_φ	K_φ
$\frac{B_\varphi}{A_\varphi}$	$\left(\frac{1}{\tau_{\varphi_1}} + \frac{1}{\tau_{\varphi_2}}\right)$	$2\zeta_\varphi\omega_\varphi$
$\frac{C_\varphi}{A_\varphi}$	$\frac{1}{\left(\tau_{\varphi_1}\tau_{\varphi_2}\right)}$	$\omega_\varphi^{\,2}$

APPENDIX B

EQUIVALENT DERIVATIVE GENERATION BY IDEAL RATE FEEDBACK AND CONTROL CROSSFEED

Total aileron input can be expressed by

$$\delta_{a_t} = \delta_{a_P} + \delta_{a_{SAS}}$$

and total rudder by

$$\delta_{r_t} = \delta_{r_P} + \delta_{r_{SAS}} + \delta_{r_{K_I}}$$

For ideal rate feedback the roll and yaw gain can be expressed by

$$K_p = -\frac{\delta_{a_{SAS}}}{p}$$

$$K_r = \frac{\delta_{r_{SAS}}}{r}$$

The aileron-to-rudder interconnect can be expressed by

$$K_I = -\frac{\delta_{r_{K_I}}}{\delta_{a_t}}$$

The total aileron and rudder can now be expressed in terms of rolling and yawing angular rates, roll and yaw SAS gains, and interconnect ratio as

$$\delta_{a_t} = \delta_{a_P} - K_p p$$

$$\delta_{r_t} = \delta_{r_P} + K_r r - K_I \left(\delta_{a_P} - K_p p\right)$$

By substituting these expressions into the equations of motion of appendix A for δ_a and δ_r, the following total and effective derivatives were obtained:

$$L_{p_t} = L_p - K_p \left(L_{\delta_a} - K_I L_{\delta_r}\right)$$

APPENDIX B

$$N_{p_t} = N_p - K_p\left(N_{\delta_a} - K_I N_{\delta_r}\right)$$

$$L_{r_t} = L_r + K_r L_{\delta_r}$$

$$N_{r_t} = N_r + K_r N_{\delta_r}$$

$$\left(L_{\delta_a}\right)_{eff} = L_{\delta_a} - K_I L_{\delta_r}$$

$$\left(N_{\delta_a}\right)_{eff} = N_{\delta_a} - K_I N_{\delta_r}$$

$$\left(Y_{\delta_a}\right)_{eff} = Y_{\delta_a} - K_I Y_{\delta_r}$$

Both the transfer-function numerator and denominator will be changed by the addition of rate feedback and control crossfeed. The total rotary derivatives and effective control derivatives should be used where applicable. However, the effective derivative is approximate and considers only an ideal system. When system characteristics such as nonlinearities, actuator dynamics, and system lead-lag filters influence handling qualities, they must also be included in a handling-qualities analysis.

REFERENCES

1. Holleman, Euclid C.: Stability and Control Characteristics of the M2-F2 Lifting Body Measured During 16 Glide Flights. NASA TM X-1593, 1968.

2. Taylor, Lawrence W., Jr.: Analysis of a Pilot-Airplane Lateral Instability Experienced With the X-15 Airplane. NASA TN D-1059, 1961.

3. Ashkenas, Irving L.; Jex, Henry R.; and McRuer, Duane T.: Pilot-Induced Oscillations: Their Cause and Analysis. TR-239-2, Systems Technology, Inc., June 20, 1964.

4. Meeker, J. I.: Evaluation of Lateral-Directional Handling Qualities of Piloted Reentry Vehicles Utilizing Fixed-Base and In-Flight Evaluations. Cornell Aero. Lab., Inc. (NASA CR-778), 1967.

5. Newell, F. D.: Ground Simulator Evaluations of Coupled Roll-Spiral Mode Effects on Aircraft Handling Qualities. Tech. Rep. AFFDL-TR-65-39, Air Force Flight Dynamics Lab., Wright-Patterson Air Force Base, March 1965.

6. Anon.: Analysis of Several Handling Quality Topics Pertinent to Advanced Manned Aircraft. Tech. Rep. AFFDL-TR-67-2, Air Force Flight Dynamics Lab., Wright-Patterson Air Force Base, June 1967.

7. Ashkenas, Irving L.; and McRuer, Duane T.: Approximate Airframe Transfer Functions and Application to Single Sensor Control Systems. Tech. Rep. 58-82 (ASTIA No. AD 151025), Wright Air Dev. Center, U.S. Air Force, June 1958.

8. Grantham, William D.; Moore, Frederick L.; Deal, Perry L.; and Patton, James M., Jr.: Simulator Study of Coupled Roll-Spiral Mode Effects on Lateral-Directional Handling Qualities. NASA TN D-5466, 1970.

9. Mechtly, E. A.: The International System of Units - Physical Constants and Conversion Factors. NASA SP-7012, 1969.

10. Painter, Weneth D.; and Kock, Berwin M.: Operational Experiences and Characteristics of the M2-F2 Lifting Body Flight Control System. NASA TM X-1809, 1969.

11. Harper, Robert P., Jr.; and Cooper, George E.: A Revised Pilot Rating Scale for the Evaluation of Handling Qualities. AGARD C. P. No. 71, Stability and Control. Part 1, Sept. 1966, pp. 227-245.

12. Mort, Kenneth W.; and Gamse, Berl: Full-Scale Wind-Tunnel Investigation of the Aerodynamic Characteristics of the M2-F2 Lifting-Body Flight Vehicle. NASA TM X-1588, 1968.

13. Conkwright, Nelson Bush: Introduction to the Theory of Equations. Ginn and Company, c. 1941.

14. Chalk, C. R.; and Wilson, R. K.: Airplane Flying Qualities Specification Revision. J. Aircraft, vol. 6, no. 3, May-June 1969, pp. 232-239.

15. Meeker, James I.; and Hall, G. Warren: In-Flight Evaluation of Lateral-Directional Handling Qualities for the Fighter Mission. Tech. Rep. AFFDL-TR-67-98, Air Force Flight Dynamics Lab., Wright-Patterson Air Force Base, Oct. 1967.

TABLE 1. PHYSICAL CHARACTERISTICS OF THE M2-F2 VEHICLE

Body –	
Planform area, meters^2 (feet^2):	
Actual	14.9 (160)
Reference, S	12.9 (139)
Longitudinal length, meters (feet):	
Actual	6.76 (22.2)
Reference, $\bar{c}$	6.11 (20.0)
Span, without rudder flare, meters (feet):	
Actual	2.94 (9.63)
Reference, b	2.91 (9.54)
Aspect ratio, $\frac{b^2}{S}$, basic vehicle	0.655
Body leading-edge sweep, degrees	77
Lower flap –	
Area, meters^2 (feet^2)	1.41 (15.23)
Span, meters (feet)	1.65 (5.42)
Chord, meters (feet)	0.86 (2.81)
Deflection, degrees:	
Pilot's control authority, down	5 to 30
Pitch stability-augmentation-system authority	±5
Design hinge moment, newton-meters (inch-pounds)	7560 (67,000)
Upper flaps, two –	
Area, each, meters^2 (feet^2)	0.89 (9.57)
Span, each, meters (feet)	1.31 (4.28)
Chord, meters (feet)	0.68 (2.23)
Deflection, degrees:	
Pitch trim (symmetric travel), up	0 to -35
Pilot's aileron authority (differential upper-flap travel)	±10
Roll stability-augmentation-system authority (differential upper-flap travel)	±5
Design hinge moment, each, newton-meters (inch-pounds)	3380 (30,000)
Vertical stabilizers, two –	
Area, each, meters^2 (feet^2)	1.50 (16.10)
Height, trailing edge, meters (feet)	1.16 (3.79)
Chord, meters (feet):	
Root	2.24 (7.36)
Tip	0.79 (2.58)
Leading-edge sweep, degrees	62.3
Rudders, two –	
Area, each, meters^2 (feet^2)	0.49 (5.27)
Span, each, meters (feet)	1.28 (4.20)
Chord, meters (feet)	0.38 (1.25)
Deflection, each (outward), degrees:	
Pilot's effective control authority	±11
Yaw stability-augmentation-system authority	±4.2
Design hinge moment, each, newton-meters (inch-pounds)	2595 (23,000)
Weight, including pilot, kilograms (pounds)	2750 (6054)
Center of gravity:	
Percentage of actual length	49
Percentage of reference length	54
Planform-area loading, $\frac{W}{S}$, kilograms/meter^2 (pounds/foot^2)	196 (43.2)
Moments of inertia –	
I_X, kilogram-meter^2 (slug-foot^2)	1409 (1037)
I_Z, kilogram-meter^2 (slug-foot^2)	9150 (6745)
I_{XZ}, kilogram-meter^2 (slug-foot^2)	-813 (-598)
Inclination of the principal axis, deg	-5.9

TABLE 2. – M2-F2 COCKPIT CONTROL AND CONTROL SURFACE CHARACTERISTICS

Surface	Input	Surface rate, deg/sec (a)	Travel, pilot's control, cm (in.)	Force gradient, N/cm (lb/in.)	Breakout, N (lb)
Lower flap	Pitch stick	25	[b]±12.7 (±5)	9.97 (5.7)	±4.45 (±1)
Upper flap	Lateral stick	30	[b]±7.62 (±3)	5.78 (3.3)	±8.00 (±1.8)
Rudder	Pedal	22	±7.62 (±3)	26.3 (15)	±17.78 (±4)

[a]Rates at 80 percent design hinge moment.
[b]Measured at pilot's grip, 49.6 cm radius (19.5 in.).

TABLE 3. – RANGE OF THE RECORDED QUANTITIES

Longitudinal stick position, cm (in.) -	
Forward	11.4 (4.5)
Aft	12.4 (4.9)
Lateral stick position, cm (in.) -	
Right	7.4 (2.9)
Left	6.9 (2.7)
Rudder-pedal position, cm (in.) -	
Right	7.4 (2.9)
Left	8.1 (3.2)
Angle of attack, deg	-10 to 30
Angle of sideslip, deg	±10
Rolling velocity, deg/sec	±60
Pitching velocity, deg/sec	±40
Yawing velocity, deg/sec	±40
Pitch attitude, deg -	
Flights 1 to 15	-30 to 60
Flight 16	±60
Roll angle, deg	±90
Normal acceleration, g	-1 to 3
Lateral acceleration, g	±1.0
Longitudinal acceleration, g	±2.0, ±0.5
Upper-flap position, deg	10 to -45
Lower-flap position, deg	0 to 35
Interconnect ratio	[a]0 to -1.0
Rudder position, deg	0 to 45

[a]Linear extrapolation possible.

TABLE 4. – MODIFIED COOPER PILOT RATING SCALE USED DURING THE PROGRAM

General classification	Numerical rating	Adjective	Handling qualities	Ability to complete mission	Ability to land
Satisfactory	1	Excellent	Easy to control precisely - little corrective control required.	Yes	Yes
	2	Very good	Good response but necessitates attention for precise control.		
	3	Good	Acceptable controllability but more than desired attention generally needed.		
Unsatisfactory	4	Fair	Submarginal for normal use - requires excessive pilot attention.	Yes	Yes
	5	Poor	Controllability poor - demands constant pilot attention and continuous control inputs.	Probably	Yes
	6	Bad	Can be controlled but pilot must exercise considerable care.	Doubtful	Yes
Unacceptable	7	Very bad	Difficult to control and demands considerable pilot concentration.	No	Probably
	8	Dangerous	Controllable only with a high degree of pilot concentration and large control inputs.	No	Doubtful
	9	Very dangerous	Extremely dangerous - can be controlled only with exceptional piloting skill.	No	No
	10	Catastrophic	Uncontrollable.	No	No

TABLE 5. – M2-F2 BASIC LATERAL-DIRECTIONAL AERODYNAMIC CHARACTERISTICS

α, deg	C_{n_β}, deg^{-1}	C_{n_p}, rad^{-1}	C_{n_r}, rad^{-1}	$C_{n_{\delta_a}}$, deg^{-1}	$C_{n_{\delta_r}}$, deg^{-1}	C_{l_β}, deg^{-1}	C_{l_p}, rad^{-1}	C_{l_r}, rad^{-1}	$C_{l_{\delta_a}}$, deg^{-1}	$C_{l_{\delta_r}}$, deg^{-1}	C_{Y_β}, deg^{-1}	$C_{Y_{\delta_a}}$, deg^{-1}	$C_{Y_{\delta_r}}$, deg^{-1}
8	0.0052	0.30	-1.75	-0.00086	-0.00175	-0.0088	-0.30	0.40	0.00077	0.00042	-0.0146	0.0007	0.0010
6	.0042	.30	-1.75	-.00086	-.00176	-.0078	-.30	.40	.00077	.00043	-.0142	.0007	.0010
4	.0035	.30	-1.75	-.00082	-.00178	-.0072	-.30	.40	.00076	.00045	-.0140	.0007	.0010
2	.0031	.30	-1.75	-.00077	-.00179	-.0067	-.30	.40	.00072	.00045	-.0138	.0007	.0010
0	.0030	.30	-1.75	-.00076	-.00180	-.0065	-.30	.40	.00070	.00045	-.0138	.0007	.0010
-2	.0029	.30	-1.75	-.00076	-.00180	-.0062	-.30	.40	.00070	.00047	-.0138	.0007	.0010
-4	.0030	.30	-1.75	-.00076	-.00180	-.0060	-.30	.40	.00070	.00050	-.0138	.0007	.0010
-6	.0031	.30	-1.75	-.00076	-.00180	-.0059	-.30	.40	.00070	.00053	-.0138	.0007	.0010

TABLE 6. – M2-F2 DIMENSIONAL DERIVATIVES AND COEFFICIENTS OF THE BANK-ANGLE TRANSFER-FUNCTION NUMERATOR AND DENOMINATOR

[M = 0.48; V = 159.5 m/sec (523 ft/sec); q = 12,100 N/m^2 (253 lb/ft^2); $\frac{1}{\tau_{wo}} = 0$]

(a) Dimensional derivatives.

α, deg	K_I, deg/deg	K_p, $\frac{\text{deg}}{\text{deg/sec}}$	K_r, $\frac{\text{deg}}{\text{deg/sec}}$	L_β, sec^{-2}	L_p, sec^{-1}	L_r, sec^{-1}	N_β, sec^{-2}	N_p, sec^{-1}	N_r, sec^{-1}	L_{δ_a}, sec^{-2}	L_{δ_r}, sec^{-2}	N_{δ_a}, sec^{-2}	N_{δ_r}, sec^{-2}	Y_β, sec^{-1}	Y_{δ_a}, sec^{-1}	Y_{δ_r}, sec^{-1}
8	0	0	0	-163.1	-0.885	1.180	14.82	0.136	-0.794	14.27	7.785	-2.451	-4.987	-0.299	0.0143	0.0205
4	0	0	0	-133.5	-.885	1.180	9.975	.136	-.794	14.09	8.341	-2.337	-5.073	-.287	.0143	.0205
0	0	0	0	-120.5	-.885	1.180	8.550	.136	-.794	12.98	8.341	-2.166	-5.130	-.283	.0143	.0205
-2	0	0	0	-114.9	-.885	1.180	8.265	.136	-.794	12.98	8.712	-2.166	-5.130	-.283	.0143	.0205
-4	0	0	0	-111.2	-.885	1.180	8.550	.136	-.794	12.98	9.268	-2.166	-5.130	-.283	.0143	.0205
-6	0	0	0	-109.4	-.885	1.180	8.835	.136	-.794	12.98	9.824	-2.166	-5.130	-.283	.0143	.0205

(b) Dimensional derivatives with SAS.

α, deg	K_I, deg/deg	K_p, $\frac{\text{deg}}{\text{deg/sec}}$	K_r, $\frac{\text{deg}}{\text{deg/sec}}$	L_β, sec^{-2}	L_{p_t}, sec^{-1}	L_{r_t}, sec^{-1}	N_β, sec^{-2}	N_{p_t}, sec^{-1}	N_{r_t}, sec^{-1}	$(L_{\delta_a})_{eff}$, sec^{-2}	L_{δ_r}, sec^{-2}	$(N_{\delta_a})_{eff}$, sec^{-2}	N_{δ_r}, sec^{-2}	Y_β, sec^{-1}	$(Y_{\delta_a})_{eff}$, sec^{-1}	Y_{δ_r}, sec^{-1}
8	0.45	0.2	0.4	-163.1	-3.040	4.294	14.82	0.177	-2.789	10.77	7.785	-0.207	-4.987	-0.299	0.0051	0.0205
4	.45	.2	.4	-133.5	-2.952	4.517	9.975	.147	-2.823	10.33	8.341	-.054	-5.073	-.287	.0051	.0205
0	.45	.2	.4	-120.5	-2.730	4.517	8.550	.108	-2.846	9.22	8.341	.143	-5.130	-.283	.0051	.0205
-2	.45	.2	.4	-114.9	-2.696	4.665	8.265	.108	-2.846	9.06	8.712	.143	-5.130	-.283	.0051	.0205
-4	.45	.2	.4	-111.2	-2.646	4.888	8.550	.108	-2.846	8.81	9.268	.143	-5.130	-.283	.0051	.0205
-6	.45	.2	.4	-109.4	-2.596	5.110	8.835	.108	-2.846	8.56	9.824	.143	-5.130	-.283	.0051	.0205

(c) Transfer-function coefficients.

α, deg	K_I, deg/deg	K_p, $\frac{\text{deg}}{\text{deg/sec}}$	K_r, $\frac{\text{deg}}{\text{deg/sec}}$	A	B	C	D	E	A_φ	B_φ	C_φ	K_φ
8	0	0	0	0.949	2.146	54.27	16.01	5.007	15.69	10.67	-187.4	16.52
4	0	0	0	.949	2.134	32.60	4.897	4.145	15.44	10.86	-170.3	16.29
0	0	0	0	.949	2.131	20.30	-1.930	3.752	14.23	9.97	-149.1	15.01
-2	0	0	0	.949	2.131	15.34	-4.573	3.576	14.22	10.05	-140.7	14.98
-4	0	0	0	.949	2.131	11.38	-6.600	3.449	14.23	10.10	-128.9	15.01
-6	0	0	0	.949	2.131	7.64	-8.701	3.382	14.23	10.13	-121.2	15.01
8	0.45	0.2	0.4	0.949	6.595	62.36	81.68	19.35	10.89	31.53	131.6	11.48
4	.45	.2	.4	.949	6.532	40.66	42.26	16.25	10.37	31.19	101.7	10.91
0	.45	.2	.4	.949	6.036	27.94	18.78	14.96	9.14	28.83	101.3	9.63
-2	.45	.2	.4	.949	6.286	22.88	7.924	14.19	8.97	28.36	96.5	9.45
-4	.45	.2	.4	.949	6.256	18.74	-0.624	13.56	8.72	27.63	96.3	9.19
-6	.45	.2	.4	.949	6.225	14.82	-8.881	13.17	8.47	26.88	96.1	8.93

TABLE 7. – M2-F2 COMPUTED LATERAL-DIRECTIONAL BANK-ANGLE ZEROS, POLES, AND MODAL CHARACTERISTICS FOR THE DATA OF TABLE 6

[M 0.48; V 159.5 m/sec (523 ft/sec); q = 12,100 N/m^2 (253 lb/ft^2); $\frac{1}{\tau_{wo}}$ 0]

α, deg	K_I, deg/deg	K_p, $\frac{deg}{deg/sec}$	K_r, $\frac{deg}{deg/sec}$	$\zeta_d\omega_d$, rad/sec	$(j\omega)_d$, rad/sec	ζ_d	ω_d, rad/sec	$\lvert\varphi/\beta\rvert_d$, deg/deg	$\lvert\varphi/\beta\rvert_{RS}$, deg/deg	$\zeta_{RS}\omega_{RS}$, rad/sec	$(j\omega)_{RS}$, rad/sec	ζ_{RS}	ω_{RS}, rad/sec	P, sec	$1/\tau_R$, sec^{-1}	$1/\tau_S$, sec^{-1}	$\zeta_\varphi\omega_\varphi$, rad/sec	$(j\omega)_\varphi$, rad/sec	$1/\tau_{\varphi_1}$, sec^{-1}	$1/\tau_{\varphi_2}$, sec^{-1}
8	0	0	0	-0.9832	7.45	0.13	7.52	3.2	673.0	-0.1477	0.268	0.48	0.309	23.5	----	-----	------	----	-3.154	3.795
4	0	0	0	-1.053	5.73	.18	5.82	4.4	402.0	-.0721	.352	.20	.359	17.9	----	-----	------	----	-3.010	3.674
0	0	0	0	-1.180	4.48	.26	4.64	6.3	258.0	.0575	.425	-.13	.429	14.8	----	-----	------	----	-2.927	3.589
-2	0	0	0	-1.284	3.89	.31	4.10	7.8	203.8	.1609	.446	-.34	.474	14.1	----	-----	------	----	-2.833	3.500
-4	0	0	0	-1.412	3.37	.39	3.65	9.7	163.8	.2893	.434	-.55	.522	14.5	----	-----	------	----	-2.698	3.368
-6	0	0	0	-1.598	2.86	.49	3.28	12.4	132.4	.4756	.324	-.83	.576	19.4	----	-----	------	----	-2.606	3.279
8	0.45	0.2	0.4	-2.741	7.05	0.36	7.57	3.2	-----	-------	-----	----	-----	----	-1.16	-0.306	-1.429	3.15	-----	------
4	.45	.2	.4	-2.856	5.25	.48	5.97	4.2	80.0	-0.586	0.370	0.85	0.693	17.0	----	-----	-1.486	2.74	-----	------
0	.45	.2	.4	-3.003	3.99	.60	5.00	5.8	55.6	-.321	.727	.40	.795	8.6	----	-----	-1.559	2.92	-----	------
-2	.45	.2	.4	-3.222	3.45	.68	4.72	6.6	46.9	-.091	.814	.11	.820	7.7	----	-----	-1.562	2.86	-----	------
-4	.45	.2	.4	-3.425	3.02	.75	4.56	7.3	41.9	.129	.818	-.16	.828	7.7	----	-----	-1.565	2.91	-----	------
-6	.45	.2	.4	-3.638	2.63	.81	4.49	8.2	38.8	.357	.750	-.43	.830	8.4	----	-----	-1.568	2.96	-----	------

TABLE 8. – M2-F2 COMPUTED LATERAL-DIRECTIONAL BANK-ANGLE ZEROS AND POLES INCLUDING ROLL AND YAW WASHOUT

[M = 0.48; K_p = 0.2; K_r = 0.4; K_I = 0.45; V = 159.5 m/sec (523 ft/sec); q = 12,100 N/m^2 (253 lb/ft^2); $\frac{1}{\tau_{wo}}$ = 0.5714 sec^{-1}]

α, deg	$\zeta_d\omega_d$, rad/sec	$(j\omega)_d$, rad/sec	$\zeta_{RS}\omega_{RS}$, rad/sec	$(j\omega)_{RS}$, rad/sec	$1/\tau_R$, sec^{-1}	$1/\tau_S$, sec^{-1}	$\zeta_{wo}\omega_{wo}$, rad/sec	$(j\omega)_{wo}$, rad/sec	$1/\tau_{wo_1}$, sec^{-1}	$1/\tau_{wo_2}$, sec^{-1}	K_φ	$1/\tau_{\varphi_1}$, sec^{-1}	$1/\tau_{\varphi_2}$, sec^{-1}	$\zeta_\varphi\omega_\varphi$, rad/sec	$(j\omega)_\varphi$, rad/sec
6	2.701	5.82	------	-----	-1.498	-0.644	-0.140	0.136	------	------	10.80	-0.679	-0.5714	-1.271	2.47
4	2.884	5.05	------	-----	-1.289	-.645	-.163	.159	------	------	10.37	-.633	-.5714	-1.474	2.51
2	2.908	4.32	-0.818	0.116	------	------	-.204	.185	------	------	9.53	-.629	-.5714	-1.528	2.66
0	3.016	3.76	-.469	.430	------	------	-.350	.159	------	------	9.14	-.628	-.5714	-1.549	2.71
-2	3.345	3.20	-.158	.676	------	------	------	-----	-0.485	-0.275	8.79	-.630	-.5714	-1.551	2.64

TABLE 9. – M2-F2 COEFFICIENTS AND ROOTS OF THE CHARACTERISTIC EQUATION FOR VARIATIONS OF C_{n_p}

[M = 0.48; K_I = 0.45; V = 159.5 m/sec (523 ft/sec); q = 12,100 N/m^2 (253 lb/ft^2); $\frac{1}{\tau_{wo}}$ = 0; α = -2°]

K_p, $\frac{deg}{deg/sec}$	K_r, $\frac{deg}{deg/sec}$	C_{n_p}, rad^{-1}	N_p	N_{p_t}	A	B	C	D	E	$\zeta_d\omega_d$, rad/sec	$(j\omega)_d$, rad/sec	$\zeta_{RS}\omega_{RS}$, rad/sec	$(j\omega)_{RS}$, rad/sec	$\lvert\varphi/\beta\rvert_d$, deg/deg	$\lvert\varphi/\beta\rvert_{RS}$, deg/deg	$1/\tau_R$, sec^{-1}	$1/\tau_S$, sec^{-1}
0	0	-0.75	-0.3402	-------	0.949	1.879	16.01	50.50	5.694	0.422	4.33	------	-----	6.5	----	-2.707	-0.117
0	0	-.25	-.1134	-------	.949	2.010	15.78	24.35	4.684	-.238	3.93	------	-----	8.0	----	-1.418	-.224
0	0	0	0	-------	.949	2.075	15.67	11.27	4.179	-.715	3.82	-0.379	0.384	8.4	264	------	------
0	0	.30	.1361	-------	.949	2.131	15.34	-4.57	3.357	-1.284	3.89	.161	.446	7.8	204	------	------
0.2	0.4	-0.75	-0.3402	-0.3579	0.949	5.988	25.11	61.89	16.01	-1.199	3.82	------	-----	7.2	----	-3.621	-0.291
.2	.4	-.25	-.1134	-.1311	.949	6.119	24.04	35.80	15.00	-2.105	3.23	------	-----	8.8	----	-1.553	-.686
.2	.4	0	0	-.0177	.949	6.184	23.51	22.70	14.50	-2.723	3.27	-0.536	0.747	7.8	46.7	------	------
.2	.4	.30	.1361	.108	.949	6.286	22.88	7.94	14.19	-3.222	3.45	-.091	.814	6.6	46.9	------	------

TABLE 10. – M2-F3 DIMENSIONAL DERIVATIVES, COEFFICIENTS OF THE BANK-ANGLE TRANSFER FUNCTION, ZEROS, POLES, AND RESPONSE CHARACTERISTICS

[M = 0.48; K_p = 0.2; K_r = 0.4; K_I = 0; q = 12,100 N/m^2 (253 lb/ft^2); $\frac{1}{\tau_{wo}}$ = 0]

(a) Dimensional derivatives.

α, deg	L_β, sec^{-2}	L_{p_t}, sec^{-1}	L_{r_t}, sec^{-1}	N_β, sec^{-2}	N_{p_t}, sec^{-1}	N_{r_t}, sec^{-1}	L_{δ_a}, sec^{-2}	L_{δ_r}, sec^{-2}	N_{δ_a}, sec^{-2}	N_{δ_r}, sec^{-2}	Y_β, sec^{-1}	Y_{δ_a}, sec^{-1}	Y_{δ_r}, sec^{-1}
8	-163.1	-3.74	4.29	14.82	0.0130	-2.79	14.27	7.79	0.616	-4.99	-0.299	0.0143	0.0205
4	-133.5	-3.70	4.52	9.98	.0403	-2.82	14.09	8.34	.479	-5.07	-.287	.0143	.0205
0	-120.5	-3.48	4.52	8.55	.0791	-2.85	12.98	8.34	.285	-5.13	-.283	.0143	.0205
-2	-114.9	-3.48	4.67	8.27	.0540	-2.85	12.98	8.71	.410	-5.13	-.283	.0143	.0205
-4	-111.2	-3.48	4.89	8.55	.0403	-2.85	12.98	9.27	.479	-5.13	-.283	.0143	.0205
-6	-109.4	-3.48	5.11	8.84	.0103	-2.85	12.98	9.82	.616	-5.13	-.283	.0143	.0205

(b) Transfer-function coefficients.

α, deg	A	B	C	D	E	A_φ	B_φ	C_φ	K_φ
8	0.949	7.201	64.88	118.7	20.79	13.92	44.15	316.5	14.70
4	.949	7.222	43.20	63.93	17.09	13.81	43.90	210.0	14.57
0	.949	7.041	30.18	28.63	15.34	12.81	40.04	150.5	13.51
-2	.949	7.040	25.35	20.65	14.68	12.74	40.73	160.0	13.43
-4	.949	7.051	21.45	14.13	14.12	12.70	41.19	170.0	13.40
-6	.949	7.055	17.84	9.49	13.87	12.62	42.00	188.0	13.32

(c) Response characteristics.

α, deg	$\zeta_d\omega_d$, rad/sec	$(j\omega)_d$, rad/sec	ζ_d	ω_d, rad/sec	$\lvert\varphi/\beta\rvert_d$, deg/deg	$\lvert\varphi/\beta\rvert_{RS}$, deg/deg	$\zeta_{RS}\omega_{RS}$, rad/sec	$(j\omega)_{RS}$, rad/sec	ζ_{RS}	ω_{RS}, rad/sec	P, sec	$1/\tau_R$, sec^{-1}	$1/\tau_S$, sec^{-1}	$\zeta_\varphi\omega_\varphi$, rad/sec	$(j\omega)_\varphi$, rad/sec
8	-2.700	6.99	0.36	7.50	3.3	----	-------	-----	----	-----	----	-1.99	-0.196	-1.567	4.49
4	-2.865	5.10	.49	5.85	4.4	----	-------	-----	----	-----	----	-1.54	-.342	-1.570	3.55
0	-3.177	3.78	.64	4.94	6.1	44.8	-0.5330	0.616	0.65	0.815	10.2	-----	------	-1.544	3.04
-2	-3.301	3.11	.73	4.54	7.3	37.2	-.4082	.765	.47	.867	8.2	-----	------	-1.580	3.15
-4	-3.463	2.51	.81	4.28	8.9	32.1	-.2529	.866	.28	.902	7.3	-----	------	-1.603	3.27
-6	-3.609	1.82	.81	4.04	11.6	28.2	-.1084	.939	.12	.946	6.7	-----	------	-1.645	3.47

TABLE 11. – M2-F3 COMPUTED BANK-ANGLE-TO-AILERON TRANSFER-FUNCTION ZEROS AND POLES WITH YAW WASHOUT FILTER

[M = 0.48; K_I = 0; V = 159.5 m/sec (523 ft/sec); q = 12,100 N/m^2 (253 lb/ft^2); $\frac{1}{\tau_{wo}}$ = 0.5714 sec^{-1}]

α, deg	K_p, $\frac{deg}{deg/sec}$	K_r, $\frac{deg}{deg/sec}$	$\zeta_d\omega_d$, rad/sec	$(j\omega)_d$, rad/sec	$\zeta_{RS}\omega_{RS}$, rad/sec	$(j\omega)_{RS}$, rad/sec	$1/\tau_R$, sec^{-1}	$1/\tau_S$, sec^{-1}	$1/\tau_{wo_1}$, sec^{-1}	K_φ	$1/\tau_{\varphi_1}$, sec^{-1}	$\zeta_\varphi\omega_\varphi$, rad/sec	$(j\omega)_\varphi$, rad/sec
6	0.2	0.4	-2.656	5.81	------	-----	-2.011	-0.536	-0.0599	14.72	-0.634	-1.420	3.720
4	.2	.4	-2.892	4.99	------	-----	-1.660	-.669	-.0691	14.55	-.617	-1.566	3.369
2	.2	.4	-3.007	4.22	-0.975	0.463	------	------	-.0789	13.81	-.625	-1.557	3.078
0	.2	.4	-3.271	3.63	-.680	.840	------	------	-.0883	13.50	-.633	-1.532	2.832
-2	.2	.4	-3.470	2.96	-.482	1.059	------	------	-.0857	13.42	-.629	-1.570	2.946
-2	.4	.4	------	----	-1.434	1.175	[a]-5.153	[a]-2.602	-.0523	13.42	-.629	-1.570	2.946

[a]Real Dutch roll roots.